Two-Charged-Particle Final States from π^-+p Interactions at 2.7 GeV/c*†

D. H. MILLER, L. GUTAY, P. B. JOHNSON, F. J. LOEFFLER, R. L. MCILWAIN, R. J. SPRAFKA,* AND R. B. WILLMANN

Department of Physics, Purdue University, Lafayette, Indiana

(Received 25 July 1966)

A total of 24 360 events having two charged particles in the final state from π^-+p interactions at an incident π^- momentum of 2.7 GeV/c have been analyzed. The final states $\pi^-\pi^+n$ and $\pi^-\pi^0p$ are found to be dominated by rho-meson production, and in addition, significant $N^*(1238)$ production is seen. The partial cross sections for the dominant resonant channels are $\sigma=(p\rho^-)=(1.3\pm0.2)$ mb, $\sigma(n\rho^0)=(2.3\pm0.2)$ mb, and $\sigma[\pi^-N^{*+}(\rightarrow p\pi^0)]=(0.5\pm0.2)$ mb. The production of the ρ^- and ρ^0 and the decay of the ρ^- agree very well with the predictions of an absorption-modified one-pion-exchange model. The production angular distributions of the ρ^0 and ρ^- follow an exponential of the form Ae^{+Bt}. The results from a least-squares fit give $B(\rho^-)=9.32\pm0.08$ (GeV/c)$^{-2}$, $B(\rho^0)=10.26\pm0.06$ (GeV/c)$^{-2}$. A similar analysis for the elastic-scattering events gave $B(\text{el})=7.77\pm0.05$ (GeV/c)$^{-2}$. The ρ^0 decay distributions are asymmetric and they have been analyzed using a simple model which includes S–P-wave interference. No clear evidence is seen for a $T=0$, $J=0$ resonance at a mass near that of the ρ. The $N^*(1238)$ resonance production is found to be in agreement with the ρ-exchange model of Stodolsky and Sakurai. Indication of other resonance production with small cross section is seen, such as A_1 and A_2 production in the multiple missing neutral events. The masses and widths of the ρ^0 and ρ^- as a function of the four-momentum transfer squared to the nucleon have been determined.

I. INTRODUCTION

IN this paper further work is presented on the interaction of π^- mesons with protons at an incident π^- momentum of 2.7 GeV/c. Previous results from this experiment,[1–3] have included the analysis of interactions leading to four charged particles in the final state, or to interactions having one or more visible strange-particle decays. The current work involved the analysis of 24 360 two-prong events obtained in an exposure of 30 000 pictures from the Lawrence Radiation Laboratory 72-in. hydrogen bubble chamber.

The experimental results presented in this paper are limited to those interactions having two charged particles in the final state, and belonging to one of the five reactions listed below.

(1) $\pi^-+p\rightarrow\pi^-+p$,

(2) $\pi^-+p\rightarrow\pi^-+p+\pi^0$,

(3) $\pi^-+p\rightarrow\pi^-+p+m\pi^0$ $(m=2,3\cdots)$,

(4) $\pi^-+p\rightarrow\pi^-+\pi^++n$,

(5) $\pi^-+p\rightarrow\pi^-+\pi^++n+m\pi^0$ $(m=1,2\cdots)$.

The present experiment was undertaken in order to study in detail the production and decay characteristics of short-lived elementary particles, in particular the ρ meson. Other experiments at nearby energies[4–9] studying the same interactions have shown that reactions 2 and 4 are dominated by ρ-meson production. An interesting feature of these results was the asymmetry seen in the decay of the neutral ρ meson. Several proposals have been made to explain this observation either in terms of interference with an S-wave isotopic spin-zero resonance at a mass near that of the ρ,[10] or to interference with some S-wave background existing in this region.[11–13] Some evidence for the possible decay of an isotopic spin-zero resonance into $\pi^0+\pi^0$ has been found[14] and an indication of a decay into $\pi^-\pi^+$ has also been reported.[15] The experimental situation, however, is by no means clear. In addition to this, very specific proposals have been made about the form of the production and decay angular distributions of both the ρ^0 and the ρ^-, providing

† Work supported in part by the U. S. Atomic Energy Commission.

* Present address: Lawrence Radiation Laboratory, Berkeley, California.

[1] D. H. Miller, A. Z. Kovacs, R. L. McIlwain, T. R. Palfrey, and G. W. Tautfest, Phys. Rev. **140**, B360 (1965).

[2] P. R. Klein, R. J. Sahni, A. Z. Kovacs, and G. W. Tautfest, Phys. Rev. **150**, 1123 (1966).

[3] D. H. Miller, A. Z. Kovacs, R. L. McIlwain, T. R. Palfrey, and G. W. Tautfest, Phys. Letters **15**, 74 (1965).

[4] Saclay-Orsay-Bari-Bologna Collaboration, Nuovo Cimento **29**, 515 (1963).

[5] Saclay-Orsay-Bari-Bologna Collaboration, Nuovo Cimento **35**, 713 (1965).

[6] V. Hagopian and W. Selove, Phys. Rev. Letters **10**, 533 (1963).

[7] Zaven G. T. Guiragossian, Phys. Rev. Letters **11**, 85 (1963).

[8] V. Hagopian, W. Selove, J. Alitti, J. P. Baton, and N. Neveu-René, Phys. Rev. **145**, 1128 (1966).

[9] Aachen-Birmingham-Bonn-Hamburg-London (I.C.)-München Collaboration, Nuovo Cimento **31**, 729 (1964).

[10] Loyal Durand, III, and Yam Tsi Chiu, Phys. Rev. Letters **14**, 329 (1965).

[11] M. M. Islam and R. Piñon, Phys. Rev. Letters **12**, 310 (1964).

[12] Sharashchandra H. Patil, Phys. Rev. Letters **13**, 261 (1964).

[13] P. G. Thurnauer, Phys. Rev. Letters **14**, 985 (1965).

[14] M. Feldman, W. Frati, J. Halpern, A. Kanofsky, M. Nussbaum, S. Richert, P. Yamin, A. Choudry, S. Devons, and J. Grunhaus, Phys. Rev. Letters **14**, 869 (1965). See also I. F. Corbett, C. J. S. Damerell, N. Middlemas, D. Newton, A. B. Clegg, W. S. C. Williams, and A. S. Carroll, Nuovo Cimento **39**, 979 (1965).

[15] V. Hagopian, W. Selove, J. Alitti, L. P. Baton, M. Neveu-René, R. Gessaroli, and A. Romano, Phys. Rev. Letters **14**, 1077 (1965).

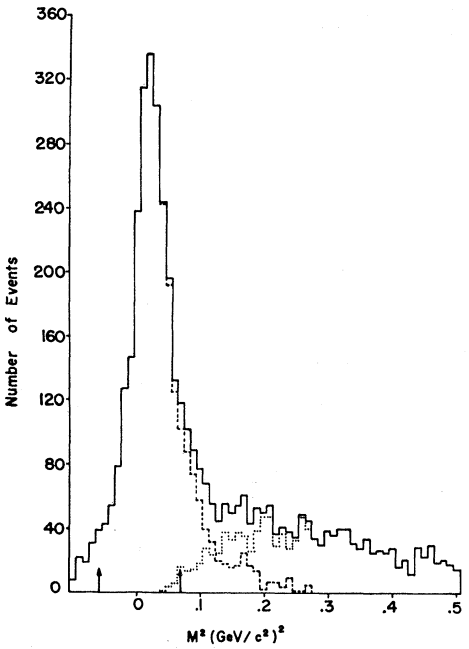

FIG. 1. Unfitted effective missing mass squared distribution from the reaction $\pi^- p \rightarrow \pi^- p +$neutrals.

that their production is dominated by one-pion exchange.[16–21]

The present experiment represents a significant increase in the number of interactions over any other single published experiment. It was therefore hoped that the analysis would yield a definitive answer on the existence of a new $T=0$ resonance, and provide a real test of the one-pion-exchange model with absorption. In addition, it was hoped to study other facets of the π^- proton interaction including those processes with small cross sections such as N^*, A_2, and A_1 production.

II. EXPERIMENTAL PROCEDURE

A. Measurement, Reconstruction, and Kinematic Fitting

The system used in measuring and reconstructing the events has been described previously[22] and consists of three scanning measuring projectors (SMP) and two measuring microscopes on line to an IBM 7044. The geometrical reconstruction and kinematical fitting were carried out on the IBM 7044 using the Berkeley PANAL-PACKAGE system. Every event classified as acceptable by this system was checked further by an additional program. This program was used to check the physical quantities and the associated errors to ensure the event had been correctly measured and also to verify that at least one physically meaningful fit had been obtained.

B. Assignment of Events

Each event passing the above tests and having a momentum for the charged secondary of less than 1250 MeV/c was examined on the scanning table to determine, with the help of the relative ionization, whether this secondary was a π^+ or a proton. Assignment of events into the five possible final states was then carried out using the value of χ^2 for each fit together with its associated probability.

In order for a given hypothesis to be considered acceptable it was necessary that it agree with the ionization information, and that the probability associated with the χ^2 for that hypothesis be greater than 1%. If the four-constraint elastic-scattering hypothesis was successful at this level the event was classified as such irrespective of the χ^2 associated with any other fits (one constraint or less). The above classification assigned unambiguously 84.5% of the events leaving 15.5% of the events ambiguous. These latter events all had two or more acceptable fits and a momentum of the positive secondary greater than 1250 MeV/c. These events fell in the main into two classes, 1392 fitted both hypothesis (4) ($\pi^-\pi^+ n$) and hypothesis (3) ($\pi^- p + m\pi^0$), while 1350 were ambiguous between (2) ($\pi^- p + m\pi^0$) and (5) ($\pi^-\pi^+ n + m\pi^0$). The members of the first class were compared, using effective-mass plots and angular distributions, with the unambiguous events already assigned to the two possible final states. It appeared from these comparisons that not more than 10% of this ambiguous

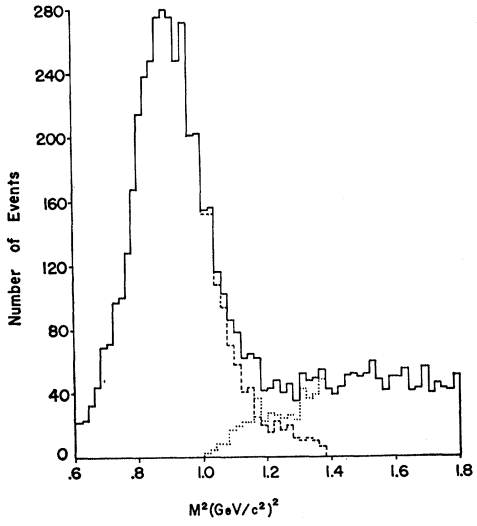

FIG. 2. Unfitted effective missing mass squared distribution from the reaction $\pi^- p \rightarrow \pi^-\pi^+ +$neutrals.

[16] A. S. Goldhaber, Phys. Rev. **134**, B600 (1965).
[17] Loyal Durand, III, and Yam Tsi Chiu, Phys. Rev. **137**, B1530 (1965).
[18] J. D. Jackson and H. Pilkuhn, Nuovo Cimento **33**, 906 (1964).
[19] J. D. Jackson, Rev. Mod. Phys. **37**, 484 (1965).
[20] J. D. Jackson, J. T. Donohue, K. Gottfried, R. Keyser, and B. E. Y. Svensson, Phys. Rev. **139**, B428 (1965).
[21] K. Gottfried and J. D. Jackson, Nuovo Cimento **34**, 735 (1964).
[22] R. L. McIlwain, IEEE Trans. Nucl. Sci. **12**, 130 (1965).

TABLE I. Partial cross sections for two-prong production in $\pi^- p$ interactions.

Final state	No. events used in analysis	Corrected cross section (mb)
$\pi^- p \to n\pi^+\pi^-$	4447	3.9 ±0.2
$p\pi^-\pi^0$	2227	2.4 ±0.2
$p\pi^-$	6416	7.7 ±0.3
$p\rho^-$		1.3 ±0.2
$n\rho^0$		2.3 ±0.2
nf^0		0.15±0.1
$\pi^- N_{1238}{}^{*+}(p\pi^0)$		0.5 ±0.2
$\pi^- N_{1688}{}^{*}(p\pi^-)$		0.1 ±0.1
$p\pi^-$ >1 neutral	2346	2.0 ±0.2
$\pi^+\pi^-$ >1 neutral	7328	7.0 ±0.3

sample belonged to hypothesis (3). All these events were, therefore, assigned to hypothesis (4) giving a background of wrongly assigned events in this channel of no more than 3% of the total sample. The second class could not be assigned so uniquely since it appeared from a similar analysis that about two-thirds of the events belonged to the state $(\pi^-\pi^+ n + m\pi^0)$ and the rest to $(\pi^- p + m\pi^0)$.

After the assignment of events as outlined above, one more source of ambiguity remained. This was the possibility that an event of the type $\pi^- p + m\pi^0$ would have an acceptable fit to hypothesis (2) $(\pi^- p\pi^0)$, or that an event of the type $\pi^-\pi^+ n + m\pi^0$ would fit $\pi^-\pi^+ n$.

Figure 1 shows a plot of the unfitted mass squared of the missing neutral system for those events having a π^- and a proton in the final state [events fitting hypothesis (1) are not included]. The solid line indicates all events, and the falling dashed line indicated those events in the overlap region acceptable as hypothesis (2). The rising

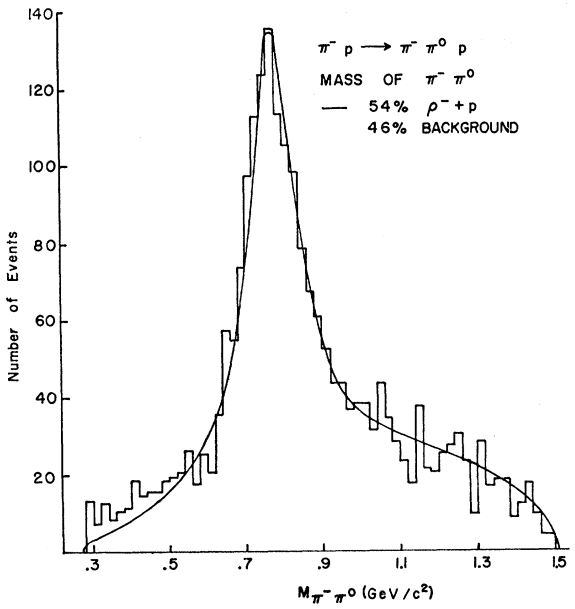

FIG. 3. Effective mass of the $\pi^-\pi^0$ system from the final state $\pi^-\pi^0 p$.

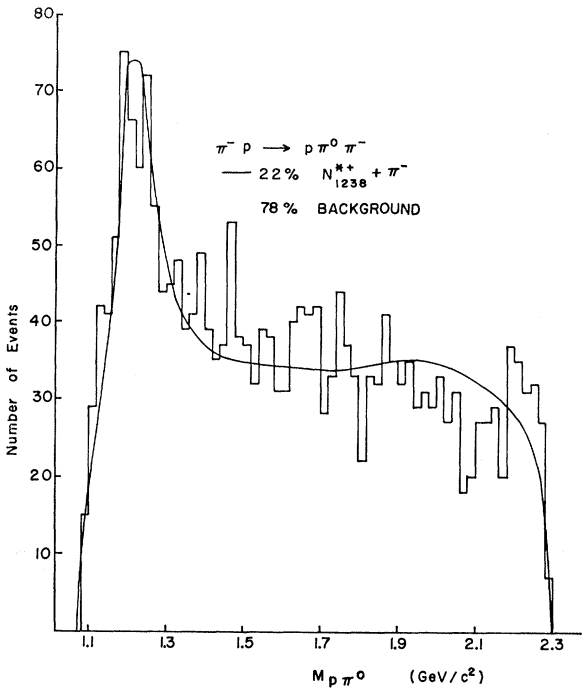

FIG. 4. Effective mass of the $p\pi^0$ system from the final state $\pi^-\pi^0 p$.

dotted line indicates those events having a probability of less than 1% of being hypothesis (2). As can be seen, some overlap occurs and this region has been excluded from the analysis of the final state $\pi^- p\pi^0$ by just using those events contained within the arrows. The events in the overlap region were compared with those within the arrows, and the fraction of true $\pi^- p\pi^0$ events excluded was estimated. The same situation is true for the events with a $\pi^-\pi^+$ in the final state as shown in Fig. 2. The overlap here is not as serious, however, and all events with a probability of greater than 1% for hypothesis (4) were used in the analysis of the final state $\pi^-\pi^+ n$. A small correction was made to the cross section for events of the type $\pi^-\pi^+ n + m\pi^0$ included in this sample.

Out of a total of 31 381 events in our fiducial volume a total of 24 360 events were accepted as having a good geometry and acceptable interpretation. The remaining events having failed, two or more measurements were examined for possible systematic deviation from the accepted sample. This sample was found to contain a larger percentage of events with lower momentum and one or more steeply dipping tracks. These biases, however, did not seem to affect our final interpretations of the data to any significant degree. These unacceptable events were used to calculate partial cross sections, being divided among the various possible final states.

III. CROSS SECTIONS

A total of 31 381 events were contained in our fiducial volume which had a total scanned pion path length of

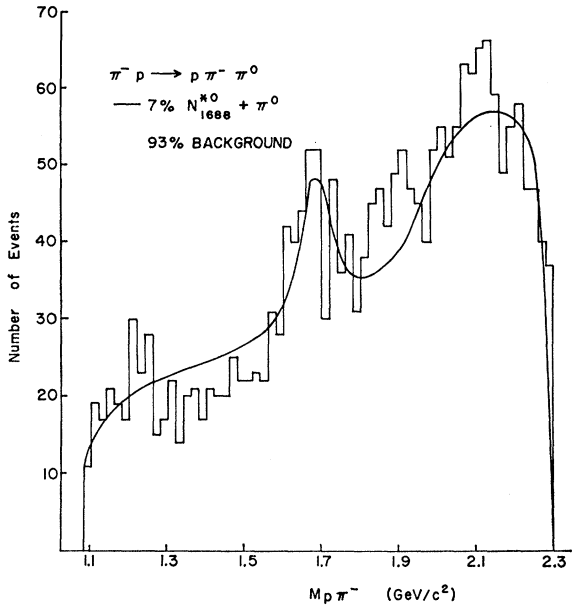

FIG. 5. Effective mass of the $p\pi^-$ system from the final state $\pi^-\pi^0 p$.

4.33×10^7 cm. This gives a total cross section for two-prong production of 22.8 ± 0.3 mb. The cross sections for the various final states are shown in Table I the main source of error coming from the allocation of events with unacceptable geometry. In addition, both the final state $p\pi^-\pi^0$ and more importantly the elastic-scattering channel have been corrected for scanning bias, i.e., for the loss of very short proton tracks. This increases the cross section and gives rise to a larger error for these channels due to the uncertainty in these correction factors.

A. Resonance-Production Cross Sections

Strong resonance production was observed in both the $p\pi^-\pi^0$ and $\pi^-\pi^+n$ final states. In order to obtain the fractions of resonance production, a least-squares-fitting procedure was used on the three possible di-particle mass projections, for each of these final states.

In the $p\pi^-\pi^0$ channel the production of two resonances could be seen; that of the ρ^- (decaying to $\pi^-\pi^0$) and the $N^*(1238)$ (decaying to $p\pi^0$). Using the Berkeley Monte Carlo program FAKE the effect of the production of these resonances on the mass projections of the other two combinations was studied. For example, a sample of events of the $p\rho^-$ was generated folding in the observed production and decay angular distributions of the ρ^-. These events were then used to determine the effect (or reflection) of this resonance production on the $p\pi^-$ and the $p\pi^0$ mass projections.

The three mass projections (Figs. 3–5), were then fitted using Breit-Wigner shapes for the resonances, with a background composed of normal phase space together with the reflection effects of the resonance production. It was found that with only two resonances the χ^2 for the $p\pi^-$ channel was large in the region of 1700 MeV/c^2. This was thought to be due to production of the $N^*(1688)$ resonance. The fit was, therefore, redone introducing this possibility. The results of the final fit are shown by the solid lines in Figs. 3–5, and as cross sections in Table I. The over-all χ^2 for each mass projection was of the order of 50 for 59 degrees of freedom. As can be seen the data are represented quite well by the over-all final fit.

A similar fitting procedure was performed on the mass projections (Figs. 6–8), of the final state $\pi^-\pi^+n$ with a few important modifications. These modifications were necessary because the only resonance observed to be produced in this channel was the ρ^0. It was expected

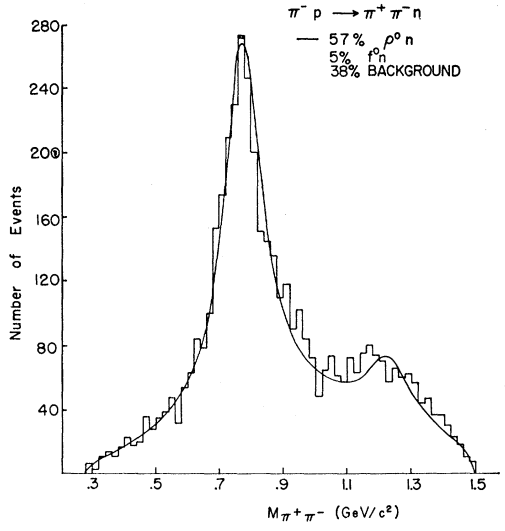

FIG. 6. Effective mass of the $\pi^-\pi^+$ system from the final state $\pi^-\pi^+n$.

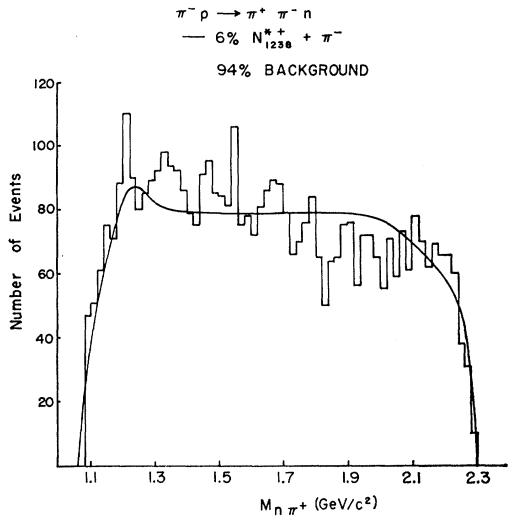

FIG. 7. Effective mass of the $n\pi^+$ system from the final state $\pi^-\pi^+n$.

that some N^* would be produced in the $n\pi^+$ decay mode which is an alternative decay mode to that already seen in the $p\pi^0$ channel. This production however, is much more difficult to observe in the $n\pi^+$ decay mode. Firstly, the relevant Clebsch-Gordan coefficients give for the decay of the N^{*+}: $\sigma(p\pi^0)/\sigma(n\pi^+)=2$; secondly, the observed cross section for the final state $n\pi^-\pi^+$ was about twice as high as for the state $p\pi^-\pi^0$. The fractional production of N^{*+} in the final state $n\pi^-\pi^+$ is, therefore, lower by a factor of 4 than that already observed in the $p\pi^-\pi^0$ final state. Lastly, the asymmetry in the ρ^0 decay leads to a large accumulation of events at low $n\pi^+$ effective mass. These events lie in the N^{*+} band and further obscure the N^{*+} production. In addition to the above the $\pi^-\pi^+$ mass spectrum does not follow phase space above 1 GeV/c^2; this is partly due to f^0 production but a significant distortion of the mass spectrum still exists even allowing for the f^0 decay. A least-squares fit was made to the $\pi^-\pi^+$ mass spectrum including the production of ρ^0 and f^0. The fit which gave the best χ^2 in the region of the ρ was chosen because of the dominance of its production. No fit was made to the $n\pi^-$ and $n\pi^+$ channels although the solid lines shown in Figs. 6–8 include the effect of N^{*+} production amounting to 50% of that found for the $p\pi^0$ decay mode. In the above analysis nominal masses and widths were used for the resonances as shown in Table II.

IV. ELASTIC SCATTERING

A total sample of 6416 events was accepted for analysis as being of the type $\pi^-+p\rightarrow\pi^-+p$. This reaction involving a four-constraint fit is very free from sources of ambiguity. The majority of the elastic-scattering events involve a low-laboratory-momentum proton in the final state, and this does lead to a serious bias. These low-momentum protons give rise to very short tracks in the bubble chamber and the bias occurs because of the difficulty in detecting these tracks and a consequent loss of such events at the scanning stage. This bias appears in the center-of-mass system of the π^-+p as an increasing loss of events as cosθ^* (where θ^* is the angle of the proton) approaches 1.0. As the interactions are viewed from one side of the chamber only, this bias is least for those events whose scattering plane lies parallel to the plane of the cameras and is maximum when it is perpendicular to this position. If we define the angle ϕ as the angle between the perpendicular to the production plane and the perpendicular to the plane of the cameras we would expect the number of events in $d\phi$ to be constant for all values of ϕ if no loss of events occured. The experimental plots of number of events versus ϕ for various values show increasing deviations from isotropy as cosθ^* approaches 1.0. These deviations were used to estimate the number of events lost. Figure 9 shows the results of this analysis in terms of the factor F by which an observed number of events at a particular center-of-mass angle θ^* should be multiplied to give the true number produced at that angle. The error bars indicate the statistical uncertainties

TABLE II. Masses and widths used in fitting the diparticle mass distributions.

Resonance	Width (MeV)	Mass (MeV)
ρ^0	150	770
ρ^-	150	770
f^0	130	1230
N^*	130	1210
N^*	100	1688

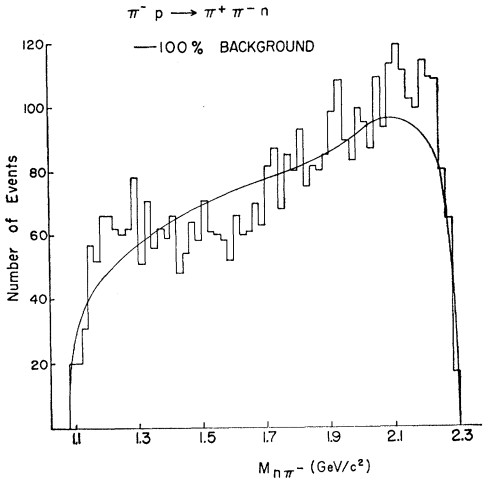

FIG. 8. Effective mass of the $n\pi^-$ system from the final state $\pi^-\pi^+n$.

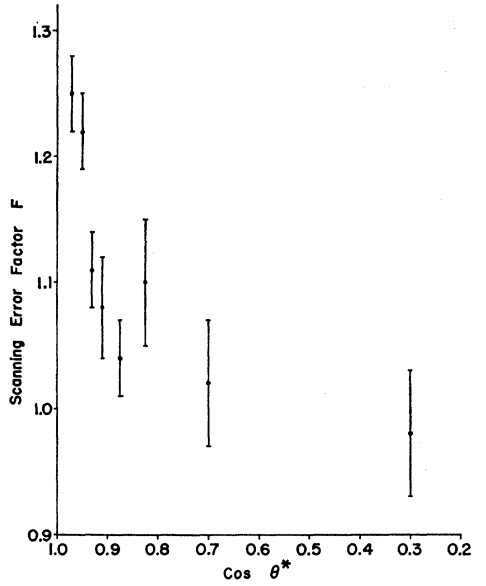

FIG. 9. F is the experimentally determined factor by which an observed number of elastic scatterings should be multiplied to obtain the true number as a function of cosθ^*, where θ^* is the center-of-mass scattering angle for the π^-. The observational loss is due primarily to scanning bias.

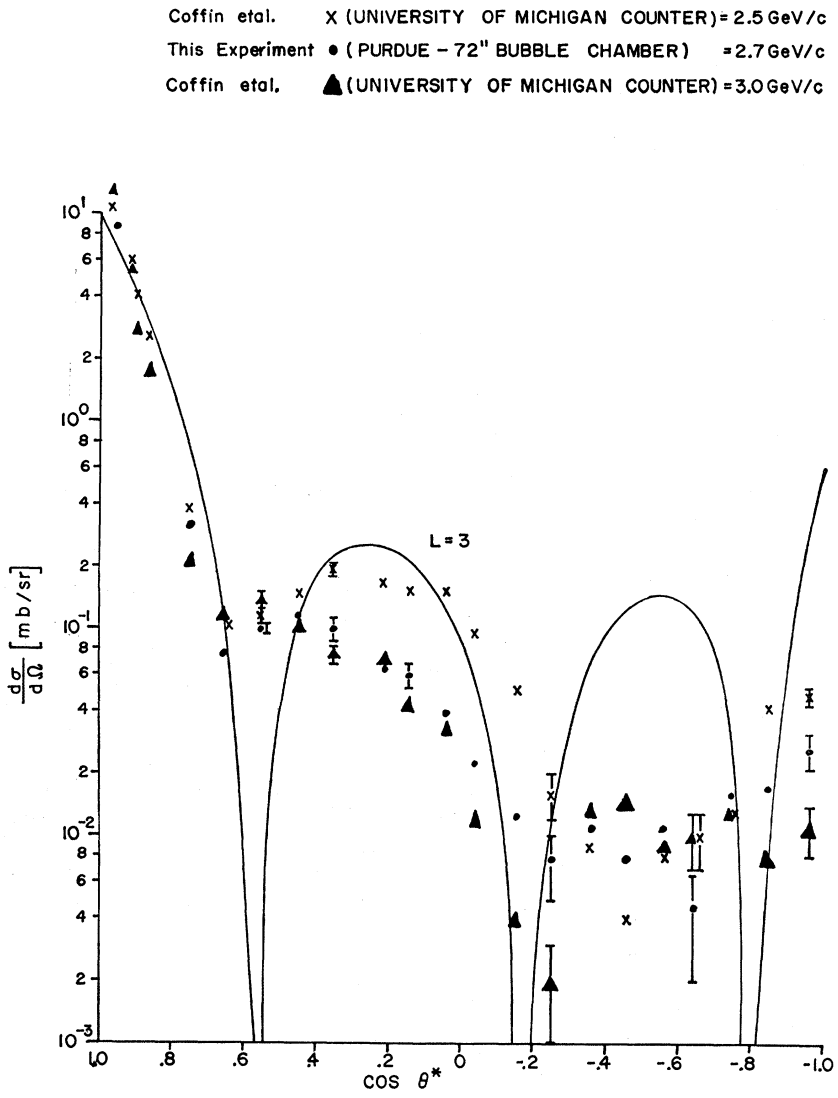

FIG. 10. Differential cross section for elastic scattering as a function of the center-of-mass scattering angle θ^* of the π^-. The bubble-chamber data from this experiment has been corrected at forward angles by the factor F of Fig. 9. The error bars on these data points represent statistical errors. The counter results of Ref. 23 are shown for comparison. For scattering more forward than $\cos\theta^* = 0.6$ only every third point from the counter data is plotted.

inherent in this procedure. This correction technique is reliable up to a $\cos\theta^*$ value of about 0.98 where serious losses begin to occur at all values of ϕ. Correction factors between $0.98 \rightarrow 1.0$ were obtained by interpolation using the last reliable factor from the above analysis and an optical-model point at $\cos\theta^* = 1.0$.

When these corrections to the data are made, the angular distribution shown in Fig. 10 is obtained. Displayed for comparison in this figure are the results of a counter experiment[23] at slightly lower and higher beam momenta, with absolute normalization. The optical-model point shown at $\cos\theta^* = 1$ was calculated assuming only an imaginary part to the scattering amplitude and a total $\pi^- p$ cross section of 32.85 mb. This value agrees well with several measurements[24] in this momentum range where the total cross section is changing very slowly with momentum. The solid curves in Fig. 10 are the prediction of a "black sphere" diffraction model[25] with a sharp cutoff for angular momentum states higher than $L = 3$. The normalization procedure for the theoretical curve was to set its total cross section equal to the value from this experiment $\sigma_{el} = 7.66$ mb.

In order to afford a further comparison with other elastic-scattering experiments, Fig. 11 depicts a number proportional to the differential cross section versus the square of the four momentum transfer, $-t$ (in units of the pion mass squared), to the nucleon. Assuming the form $d\sigma/dt = A \exp(+Bt)$, we find by a least-squares fit

[23] C. T. Coffin, N. Dikmen, L. Ettlinger, D. Meyer, A. Saulys, K. Terwilliger, and D. Williams, Phys. Rev. Letters **15**, 838 (1965).

[24] A. N. Diddens, E. W. Jenkins, F. T. Kycia, and K. F. Riley, Phys. Rev. Letters **10**, 262 (1963).

[25] L. M. Simmons, Phys. Rev. Letters **12**, 229 (1964).

to the data a value of (7.77 ± 0.05) $(\mathrm{GeV}/c)^{-2}$ for B which is in good agreement with other results.[26,9]

The results of this elastic-scattering analysis do not contribute any really new physical information, although the agreement with other data obtained by different experimental methods tends to be reassuring.

V. FINAL STATE $p\pi^-\pi^0$

A. General Features

A total sample of 2227 events was used for the analysis of the final state $p\pi^-\pi^0$. The main physical procseses occurring are exhibited in Fig. 12 where $M_{p\pi^0}{}^2$ vs $M_{\pi^-\pi^0}{}^2$ is plotted for each event. Strong production of the ρ^- can be seen and in addition a clear increase of density of points is seen in the region where the $N^{*+}(1238)$ can be produced. This latter feature had not been clearly seen prior to this experiment. The Dalitz plot of $M_{p\pi^-}{}^2$ vs $M_{\pi^-\pi^0}{}^2$ (Fig. 13) does not reveal any new resonance bands although the ρ^- and N^{*+} production can be clearly seen. The projections of the three possible di-particle masses are shown in Figs. 3–5 where the production of the above resonances can be seen as peaks. The solid lines, as has been stated, are the results of a least-squares fit to find the various partial cross sections. The $p\pi^-$ mass projection indicates the possibility of production of the $N^*(1688)$ resonance. The statistical significance, however, of the peak seen in this mass region is not large.

The reaction $\pi^-p\rightarrow p\rho^-$ occurs mainly at small values of $-t$, the square of the four momentum transfer to the proton. This is shown in Fig. 14 where $M_{\pi^-\pi^0}{}^2$ is plotted

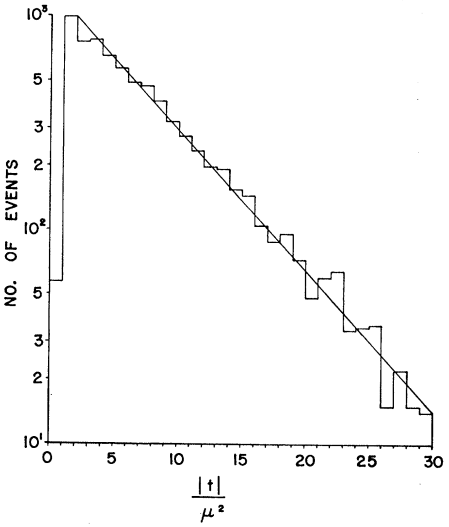

FIG. 11. Dependence of the differential cross section for elastic scattering on the invariant four-momentum transfer to the proton for small momentum transfers. The solid line is the result of a least-squares fit to the data. It has a slope of 7.77 $(\mathrm{GeV}/c)^{-2}$.

[26] Aachen-Berlin-CERN Collaboration, Phys. Letters **19**, 608 (1965).

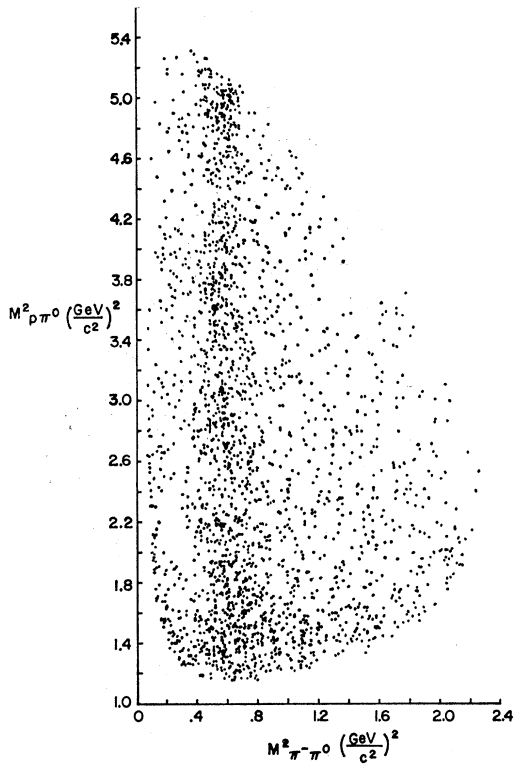

FIG. 12. Dalitz plot for the final state $\pi^-\pi^0p$.

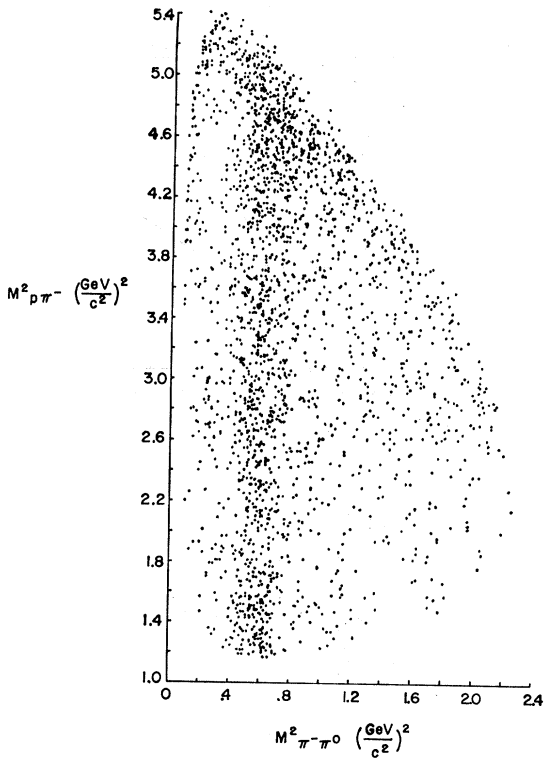

FIG. 13. Dalitz plot for the final state $\pi^-\pi^0p$.

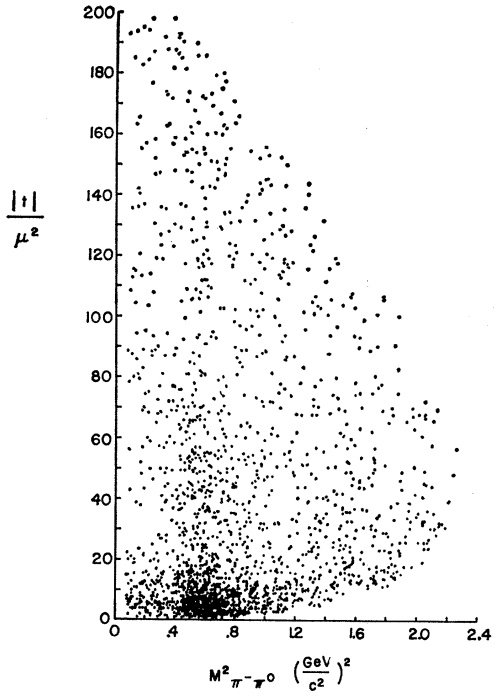

FIG. 14. Chew-Low plot of four-momentum transfer squared $(-t)$ to the $\pi^-\pi^0$ system versus $M_{\pi^-\pi^0}{}^2$ from the final state $\pi^-\pi^0 p$.

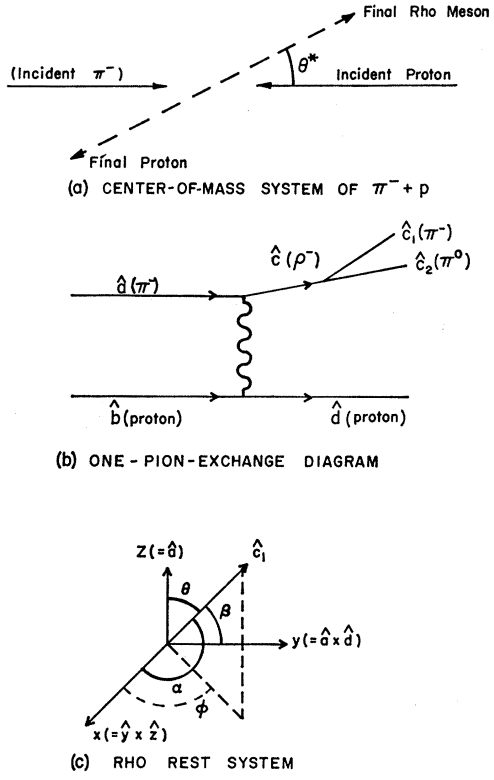

FIG. 15. Coordinate systems and definitions of angles used in the analysis of the ρ meson production and decay.

against $-t$ in units of μ^2 (the mass of the pion squared). At a mass near 0.77 GeV/c^2 a large number of events corresponding to ρ^- production can be seen clustered in the region of $-t<20\mu^2$.

B. Production and Decay of the ρ^-

In order to study the production and decay of the ρ^-, a coordinate system as shown in Fig. 15 was used. Events for which the $\pi^-\pi^0$ effective mass lay between 0.66 GeV/c^2 and 0.88 GeV/c^2 were taken as being representative of the ρ^- production and decay. From the least-squares fit to the $\pi^-\pi^0$ mass projection it was estimated that about 15% of these events did not correspond to ρ^- production. These events constituted a background which was more important in the region $-t>20\mu^2$. The total cross section for ρ^- production was known from the fits to the mass projections and the total pion path length. The events used in the ρ^- analysis were considered then to represent this cross section and the conversion between this subsample of events in the region 0.66–0.88 GeV/c^2 and a cross section was easily obtained.

The production angular distribution of the $\pi^-\pi^0$ system in the π^-p center-of-mass system for these events is shown in Fig. 16 where cross section is plotted against $\cos\theta^*$. The solid line represents the predictions of Jackson *et al.*[27] based on their calculations using the one-pion-exchange model with absorption. The curve is not a fit to the data but an absolute prediction. The solid line fits the data rather well except at $\cos\theta^*>0.96$. This

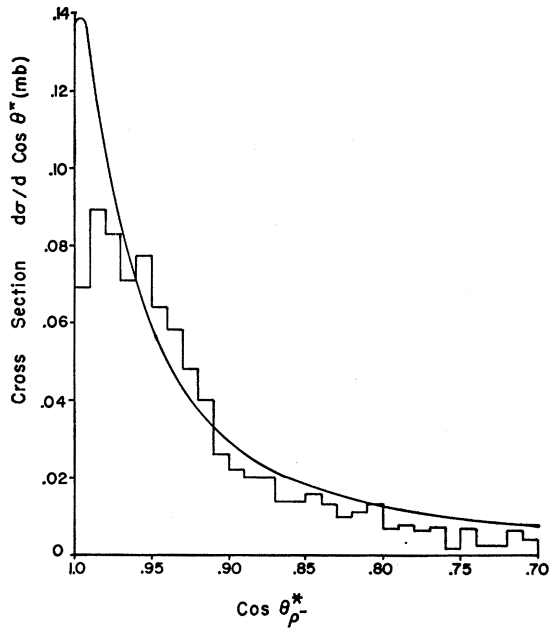

FIG. 16. $d\sigma/d(\cos\theta^*)$ for events in the $\pi^-\pi^0$ effective-mass range 0.66–0.88 (GeV/c^2).

[27] Specific calculations were made for our energy by J. D. Jackson using techniques described in Ref. 19.

is probably due to loss of events while scanning since large values of $\cos\theta^*$ correspond to low-momentum protons in the laboratory. If a significant loss of protons with projected lengths less than $3\frac{1}{2}$ mm had occurred during scanning, this discrepancy would be explained. This loss seems reasonable when one considers the analysis of our elastic-scattering events where the angular distribution is better known and the minimum observable length more easily calculated. The production angular distribution closely follows an exponential. In Fig. 17 is shown log(No. of events $\times 2$) plotted against $|t|/\mu^2$ and the solid line indicates the results of a least-squares fit in the region between the arrows. The results of this fit give $d\sigma/dt = (0.18\pm0.02)e^{+(9.32\pm0.08)t}$ mb $(\mathrm{GeV}/c^2)^{-2}$. This is very similar to that found by other workers[2,9] and to our own angular distribution for the elastic-scattering events.

The ρ^- is produced as a mixture of pure quantum-mechanical spin states which is conveniently described in terms of the spin density matrix[28] of the ρ^- with the elements $\rho_{mm'}$ (m, m' being the magnetic quantum numbers of the ρ^- running from $-J$ to J). This matrix of the $\rho^-(J=1)$ is

$$\begin{pmatrix} \rho_{11} & \rho_{10} & \rho_{1,-1} \\ \rho_{10}^* & \rho_{00} & -\rho_{10}^* \\ \rho_{1,-1} & -\rho_{10} & \rho_{11} \end{pmatrix},$$

where ρ_{00}, $\rho_{1,-1}$, and ρ_{11} are real and ρ_{10} is complex. This gives for the expected decay distribution of the

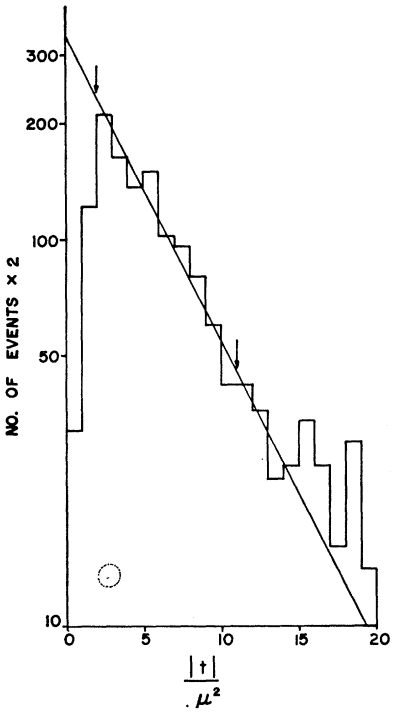

FIG. 17. Events in the ρ band were taken and shown is a plot of $\log_{10}$ (number of events $\times 2$) versus the four-momentum transfer squared to the $\pi^-\pi^0$ system in units of M_π^2, together with the results of a least-squares straight-line fit.

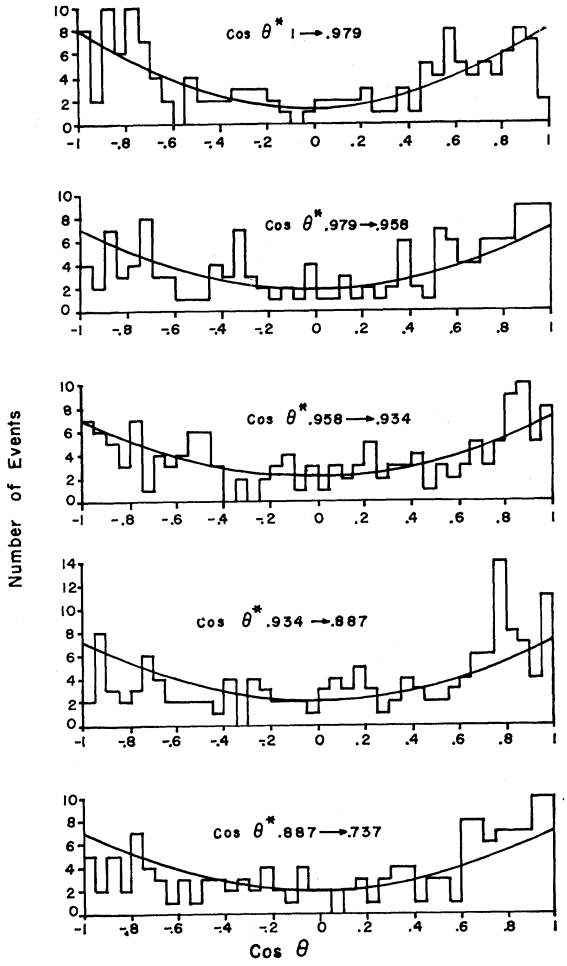

FIG. 18. Cosine of the "$\pi\pi$ scattering angle" for successive intervals of $\cos\theta_{\rho^-}{}^*$ using events with $M_{\pi^-\pi^0}$ from 0.66 to 0.88 (GeV/c^2).

$$\rho^- \rightarrow \pi^- + \pi^0,$$

$$W(\cos\theta,\phi) = (3/4\pi)[\rho_{00}\cos^2\theta + \rho_{11}\sin^2\theta - \rho_{1,-1}\sin^2\theta\cos 2\phi - \sqrt{2}\,\mathrm{Re}\rho_{1,0}\sin 2\theta\cos\phi],$$

with the trace condition that $\rho_{00} = 1-2\rho_{11}$. Integration of the above gives the distribution expected in $\cos\theta$ and ϕ

$$W(\phi) = (1/2\pi)[(1+2\rho_{1,-1}) - 4\rho_{1,-1}\cos^2\phi],$$

$$W(\cos\theta) = \tfrac{3}{4}[(1-\rho_{00}) + (3\rho_{00}-1)\cos^2\theta],$$

where θ and ϕ are angles defined in Fig. 15. The derivation of these expressions and a general treatment of the density matrix for the case of a resonance $d \rightarrow \alpha+\beta$ where α and β are particles with spin has been carried out by several authors.[29] The validity of the above expressions holds for the process under consideration irrespective of any model such as one-pion exchange (OPE) which is used to explain the production process.

[28] K. Gottfried and J. D. Jackson, Phys. Letters 8, 144 (1964).

[29] H. Pilkuhn and B. E. Y. Svensson, Nuovo Cimento **38**, 518 (1965).

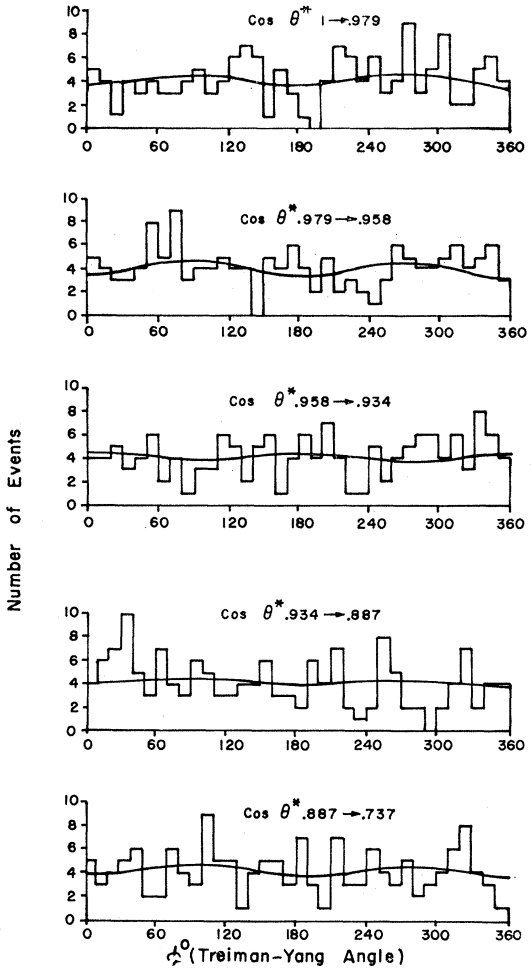

FIG. 19. The Treiman-Yang angle ϕ^0 for successive intervals of $\cos\theta_{\rho^-}$* using events with $M_{\pi^-\pi^0}$ from 0.66 to 0.88 GeV/c^2.

It does assume a decay of pure ρ^- produced in a parity-conserving interaction.

If, however, the one-pion-exchange diagram shown in Fig. 15 dominates the process $\pi^-+p\rightarrow p+\rho^-$ then specific predictions can be made about the values of $\rho_{m,m'}$. To do this we consider this process in the ρ^- rest-frame and take the direction of the incident π^- as our axis of quantization, and invoke angular-momentum conservation. As $L_z=0$ the values of $m=\pm1$ are forbidden for the magnetic projections and therefore $\rho_{\pm1,m'}$ and $\rho_{m,\pm1}$ are zero leaving just ρ_{00} nonzero and equal to one. This idealized situation is not realized in practice, the presence of other possible channels open to the π^-p interaction producing modifications. The one-pion-exchange model including these effects (absorption) has been treated in particular by Jackson and coworkers.[19,27] They have supplied us with their predictions of the values of $\rho_{m,m'}$ for the process $\pi^-p\rightarrow p\rho^-$ at an incident π^- momentum of 2.7 GeV/c. These values of $\rho_{m,m'}$ are not unique but vary with the four-momentum transfer to (or $\cos\theta^*$ of) the $\pi^-\pi^0$ system.

In order to determine the values of these matrix elements the events in the mass region 0.66–0.88 GeV/c^2 were arranged in descending order of $\cos\theta^*$ and then divided into consecutive groups of 150. For each group of events the program MINFUN was used to determine the best fit to the experimental data of the function $W(\theta,\phi)$. The projections onto the $\cos\theta$ and ϕ axes for these groups of events are shown in Figs. 18 and 19, the solid lines indicating the best fits to $W(\theta,\phi)$. The distribution in $\cos\theta$ and ϕ for $|t|<10\mu^2$ and the mass of the $\pi^-\pi^0$ system between 0.66 and 0.88 GeV/c^2 is shown in Fig. 20. Deviations from the predicted density of points as a function of (θ,ϕ) can be seen, in particular the density of points being higher for $\cos\theta>0.5$ than for $\cos\theta<0.5$. The actual values of $\rho_{m,m'}$ are shown in Fig. 21 (the points with solid-line error bars) together with the predictions of Jackson *et al.* (the continuous line). The agreement is quite reasonable particularly as no attempt has been made to include possible background effects. Undoubtedly these background effects are important particularly at lower values of $\cos\theta^*<0.7$ where the distribution in $\cos\theta$ is becoming quite asymmetric. The production of $N^*(1238)$ in the $p\pi^0$ channel gives rise to an excess of events at $\cos\theta\sim1$ and is a contributing factor in the observed asymmetry.

In order to examine these background effects two regions, one on either side of the ρ band (0.66–0.88 GeV/c^2), were taken. These regions were chosen using the results of the least-squares fit to the $\pi^-\pi^0$ mass distribution so that when combined they contained the same number of non-rho events as did the ρ band. These events were then subtracted in the fitting procedure from the events in the original band. The dotted points shown in Fig. 21 correspond to the values of $\rho_{m,m'}$ obtained using this technique. The subtraction does not affect the values significantly for $\cos\theta^*>0.8$ where the majority of the ρ production is taking place. It does lower the value of ρ_{00} at $\cos\theta^*\sim0.7$ where the back-

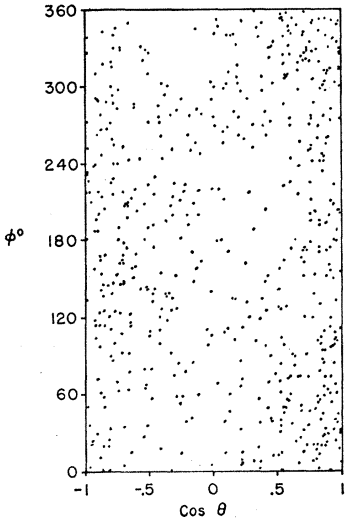

FIG. 20. $\cos\theta$ versus ϕ^0 for events with a $\pi^-\pi^0$ mass from 0.66 to 0.88 GeV/c^2 and $|t|<10\mu^2$.

ground effects are expected to be larger. The results although consistent with the OPE model with absorption are also consistent with little variation of $\rho_{m,m'}$ with four-momentum transfer. The above model does predict that $\rho_{1,-1}$ should never be negative although there is one point at $\cos\theta^*\sim 0.93$ where this does occur: a recent experiment[30] on ρ^- production also reports a negative value of $\rho_{1,-1}$ in this region. It is not clear, however, whether this represents a breakdown of the model or an inability to subtract out processes such as $N^*(1238)$ production. These processes could be important. For example, an examination of the forward-backward asymmetry parameter reveals a strong variation as a function of mass. This is shown in Fig. 22 where our experimental points are plotted for $|t|<20\mu^2$, the smooth curve indicating approximate results from previous experiments.[5] The breakup of the $\pi^-\pi^0$ system is symmetric at the ρ^- mass although in the above analysis we have used a wide band of events which introduces some asymmetry.

The determination of the density matrix elements for the decay of the $N^*(1238)$ is a little more complicated. The complications arise in general because of the much higher ratio of background to resonance, and the small production cross section. A calculation in terms of the elements $\rho_{m,m'}$ of the density matrix for the $N^*(J=\frac{3}{2})$

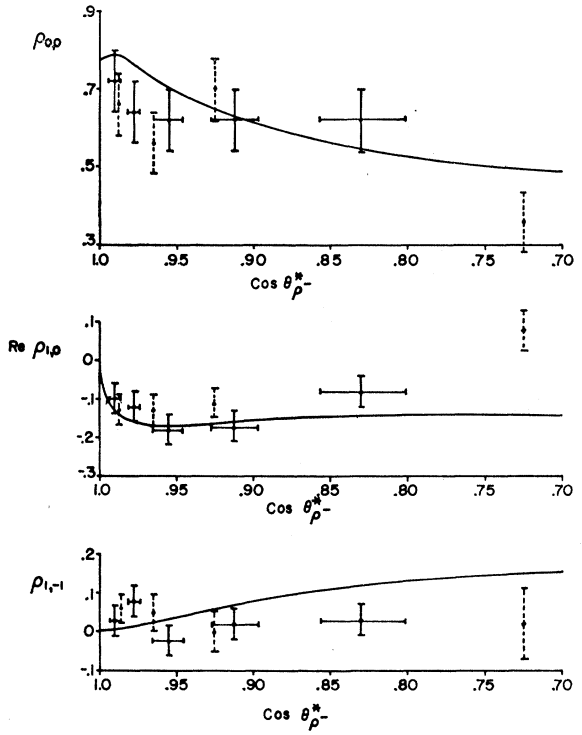

FIG. 21. Experimental density matrix elements for ρ^- decay.

[30] H. R. Bleiden, M. N. Foccaci, L. Dubal, W. Kienzle, F. Lefèbvres, B. Levrat, and B. C. Maglić, Phys. Letters **19**, 708 (1966).

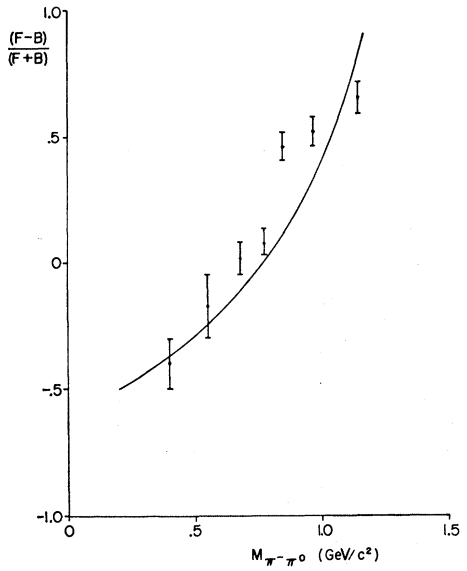

FIG. 22. Forward-backward asymmetry parameter for the $\pi^-\pi^0$ system as a function of mass for $|t|<20\mu^2$.

decay gives an expected distribution of

$$W(\theta,\phi)=(3/4\pi)\{\rho_{3/2,3/2}\sin^2\theta+\rho_{1/2,1/2}(\tfrac{1}{3}+\cos^2\theta)-(2/\sqrt{3})\,\mathrm{Re}\rho_{3/2,-1/2}\sin^2\theta\cos 2\phi-(2/\sqrt{3})\,\mathrm{Re}\rho_{3/2,1/2}\sin 2\theta\cos\phi\}$$

with the trace condition that $2\rho_{3/2,3/2}+2\rho_{1/2,1/2}=1$. Integrating over $\cos\theta$ and ϕ gives the projected distributions on these axes of

$$W(\cos\theta)=\tfrac{1}{4}[(1+4\rho_{3/2,3/2})+(3-12\rho_{3/2,3/2})\cos^2\theta],$$

$$W(\phi)=(1/2\pi)[(1+4/\sqrt{3}\,\mathrm{Re}\rho_{3/2,-1/2})-8/\sqrt{3}\,\mathrm{Re}\rho_{3/2,-1/2}\cos^2\phi].$$

The angles θ and ϕ used in the above expressions are those defined in Fig. 23(c) in the rest system of the $p\pi^0$.

The program MINFUN was once again used to find the best estimate of $W(\theta,\phi)$ using those events with a $p\pi^0$ effective mass between 1.14 and 1.28 GeV/c^2 and having $\cos\theta_{p\pi^0}^*>0.75$. Only one value of the matrix elements could be calculated in this region because of the lack of events. The values obtained are shown in Table III in column I and the distributions in Fig. 23(a) and 23(b). An attempt was made to subtract out possible back-

TABLE III. Values of the density matrix elements for the N^{*+} decay obtained by taking events in the N^* region 1.14–1.28 GeV/c^2 and events in the region 1.28–1.42 GeV/c^2 and fitting the angular distributions in the $p\pi^0$ center-of-mass system to the form $A+B\cos X+C\cos^2 X$.

	I	II	III	Predicted
$\rho_{3/2,3/2}$	0.219±0.04	0.332±0.06	0.35±0.06	0.375
$\mathrm{Re}\rho_{3/2,-1/2}$	0.124±0.04	0.197±0.05	0.25±0.05	0.22
$\mathrm{Re}\rho_{3/2,1/2}$	−0.055±0.03	−0.09 ±0.04	···	0

TABLE IV. Coefficients obtained from fitting the angular distributions in the $p\pi^0$ rest system to the form $A+B\cos X+C\cos^2 X$.[a]

	For the fits to			$A+B\cos X+C\cos^2 X$			Derived for the $N^*(1238)$		
	A	B	C	A	B	C	A^*	B^*	C^*
$\cos\theta$	0.45	0.24	0.15	0.31	0.44	0.57	0.6	0.04	−0.27
$\cos\beta$	0.39	0.03	0.33	0.56	0.08	−0.18	0.22	−0.02	0.84
ϕ	0.22	0.036	−0.12	0.19	0.015	0.06	0.25	0.05	−0.3
Mass interval (GeV/c^2)		1.14→1.28			1.28 → 1.42				
No. of events		293			200				
Estimated fraction of resonance		70%			40%				

[a] All the above for $-t<20\mu^2$ (to $p\pi^0$ system).

ground events by utilizing regions on either side of the chosen band, the results of this are tabulated in Table III column II.

An additional attempt was made to determine the decay distributions of the N^* by fitting the distributions in $\cos\theta$, $\cos\beta$, and ϕ (see Fig. 23) independently to the form $A+B\cos X+C\cos^2 X$. Two regions were taken and fitted independently, one from a mass of 1.14–1.28 GeV/c^2 and the other from 1.28–1.42 GeV/c^2. The fraction of N^* production in these bands was obtained from the fits to the $p\pi^0$ mass distributions. It was then assumed that the N^* decay could be represented by $A^*+B^*\cos X+C^*\cos^2 X$ and the background by $A'+B'\cos X+C'\cos^2 X$ with no interference. By using the known fractions of resonance and background, and the results of the fit to the distributions for the numerical values of A, B, and C for each of the two regions, A^*, B^*, and C^* can be calculated. The results are shown in Table IV. An interesting result from this analysis is that B^* is always consistent with zero. This would be expected from the free decay of a sample of N^* events and gives some justification for the procedure used. The values of $\rho_{m,m'}$ obtained are shown in column III of Table III although since we have used projections the value of $\mathrm{Re}\rho_{3/2,1/2}$ cannot be determined. The values of the other matrix elements are similar to those obtained from the other techniques.

One theoretical model which has had some success in

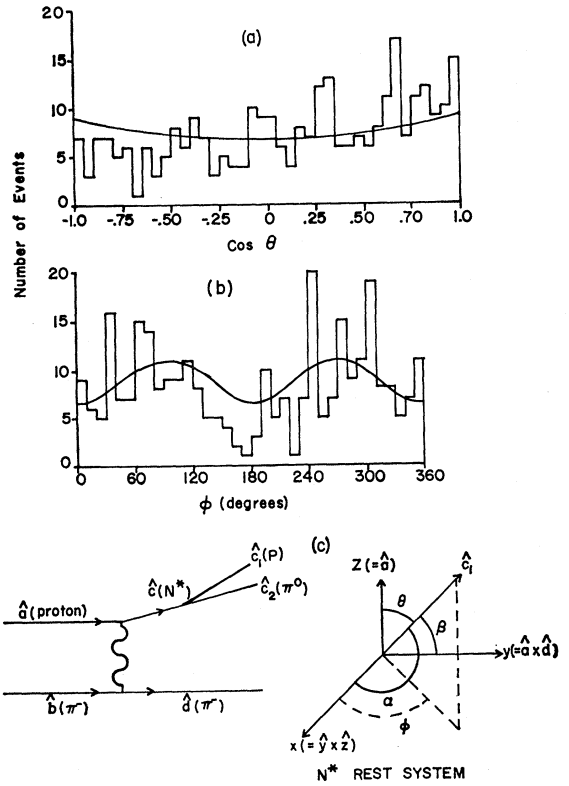

FIG. 23. (a) $\cos\theta$ for the decay of the $N^*(1238)\rightarrow p\pi^0$; (b) ϕ for the decay of the $N^*(1238)\rightarrow p\pi^0$; (c) coordinate system used for N^* analysis.

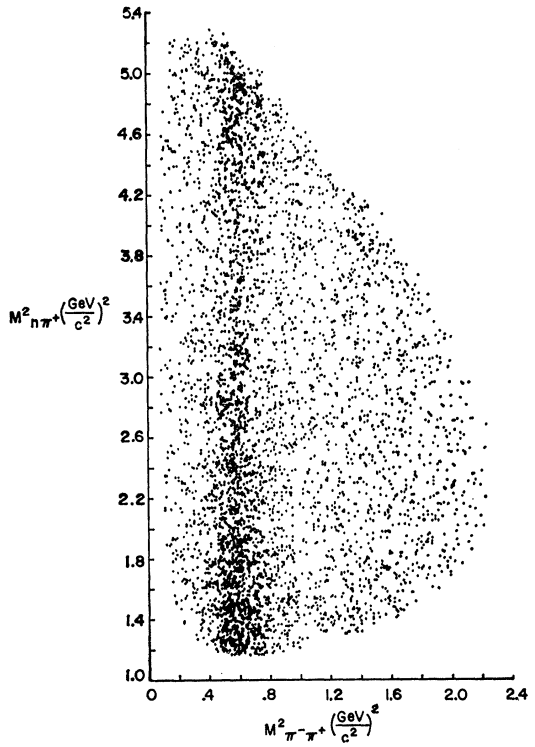

FIG. 24. Dalitz plot for the final state $\pi^-\pi^+n$.

other reactions[31,32] assumes that the final state $N^{*+}\pi^-$ is produced by ρ^0 exchange. Stodolsky and Sakurai[33,34] have given results from such a model in which they treat the $N\rho N^*$ vertex like an $N\gamma N^*$ vertex since the ρ and γ have the same quantum numbers. They predict that

$$W(\cos\theta,\phi)=(1/8\pi)(1+\sin^2\theta\sin^2\phi)$$

implying that $\rho_{3/2,3/2}=0.375$, $\mathrm{Re}\rho_{3/2,-1/2}=0.216$, and $\mathrm{Re}\rho_{3/2,1/2}=0$. These values are very similar to those obtained in columns B and C of Table IV which is some justification for using this model. The techniques used above are essentially only qualitative as several other processes such as interference may be important. The reasonably good agreement obtained between theory and experiment may indicate, however, that these effects are small.

VI. FINAL STATE $\pi^-\pi^+$n

Out of a total of 4447 events accepted and used in the analysis of the final state $\pi^-\pi^+n$, 1392 of these events were also acceptable as coming from the final state π^-pX^0. This subset of events, all with a positive secondary having a momentum greater than 1250 MeV/c, were examined separately and the distributions of effective masses and angles studied. From these studies it appeared that if all were assigned to reaction (4) only 3% of the 4447 events would have been incorrectly assigned. This has been done in the following analysis, the incorrectly assigned events not being numerous enough to affect the conclusions reached.

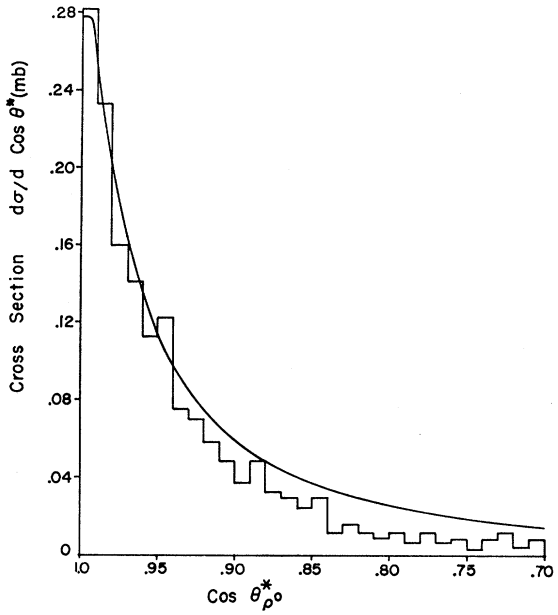

FIG. 26. $d\sigma/d(\cos\theta^*)$ for events in the $\pi^-\pi^+$ effective-mass interval 0.66 to 0.88 GeV/c^2.

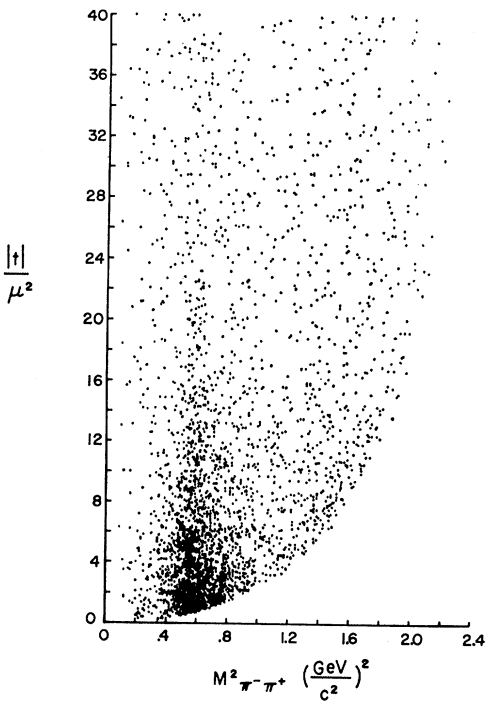

FIG. 25. Chew-Low plot of $|t|/\mu^2$ to the $\pi^-\pi^+$ system versus $M_{\pi^-\pi^+}{}^2$ from the final state $\pi^-\pi^+n$.

In Fig. 24 is shown a Dalitz plot with $M_{\pi^-\pi^+}{}^2$ plotted against $M_{n\pi^+}{}^2$. Deviations from an isotropic distribution can be seen corresponding to ρ^0 production but no other clear deviations are observed. From the observed amount of $N^*(1238)$ in the $\pi^-p\pi^0$ final state it is calculated that about 250 events should correspond on this plot to $\pi^-p\rightarrow\pi^-N^*$, $N^*\rightarrow n\pi^+$. This small number of events is very difficult to observe over the high background which is caused in large part by the ρ^0 asymmetry in decay. The three possible di-particle effective-mass plots are shown in Figs. 6–8 the solid lines indicating a least-squares fit to the data which has already been described. The $\pi^-\pi^+$ effective-mass distribution deviates strongly from phase space above 1 GeV/c^2. This is partly due to f^0 production although the peak in this region falls at a mass around 1180 MeV/c^2 compared with the normally accepted mass for the f^0 of 1250 MeV/c^2. A two-dimensional plot of $M_{\pi^-\pi^+}{}^2$ against $-t$ (four-momentum transfer squared to the neutron) in Fig. 25 reveals that the majority of ρ^0 and f^0 production occurs at $-t<20\mu^2$. The $\pi^-\pi^+$ effective-mass spectrum for $-t<20\mu^2$ has a peak around 1210 MeV/c^2 which is still a little low for the f^0. Background effects appear to be important in this region and the solid line in Fig. 6 which includes 5% f^0 production probably

[31] M. Abolins, D. Duane Carmony, Duong-N. Hoa, Richard L. Lander, C. Rindfleisch, and Nguyen-Huu Xuong, Phys. Rev. **136**, B195 (1964).
[32] Saclay-Orsay-Bologna-Bari Collaboration, Phys. Letters **13**, 341 (1964).
[33] L. Stodolsky, Phys. Rev. **134**, B1099 (1964).
[34] L. Stodolsky and J. J. Sakurai, Phys. Rev. Letters **11**, 90 (1963).

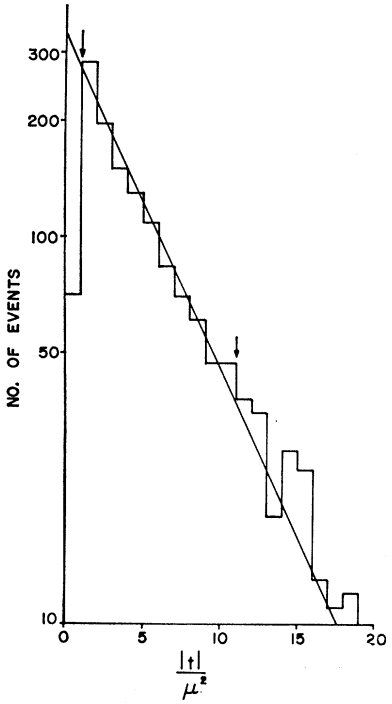

FIG. 27. Events were taken in the ρ region and shown is a plot of $\log_{10}$(number of events) versus $|t|/\mu^2$ together with the results of a least-squares straight-line fit.

represents an upper limit for the process $\pi^- p \rightarrow f^0 n$. For these reasons no attempt had been made to systematically study the f^0.

A. ρ^0 Production and Decay

The production and decay of the ρ^0 was studied using the coordinate system shown in Fig. 15 (by replacing the ρ^- by the ρ^0, the proton by a neutron, and the final π^0 by a π^+). Events were taken having a $\pi^-\pi^+$ effective mass between 0.66 and 0.88 GeV/c^2 and these were considered as being typical of ρ^0 production. The production angular distribution in the over-all center-of-mass system is shown in Fig. 26. The solid line is once again a prediction of Jackson *et al.*,[27] the only difference between this and the ρ^- production being that the cross section for ρ^0 production should be a factor of 2 larger at all values of cosθ^*. The fit is very good not only to the shape of the histogram but in absolute magnitude.

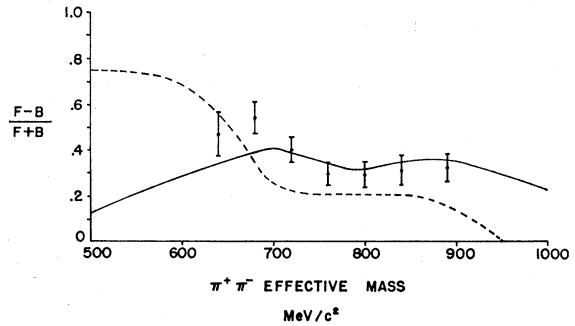

FIG. 28. Forward-backward asymmetry parameter α as a function of the effective mass of the $\pi^-\pi^+$ system for $|t|<20\mu^2$.

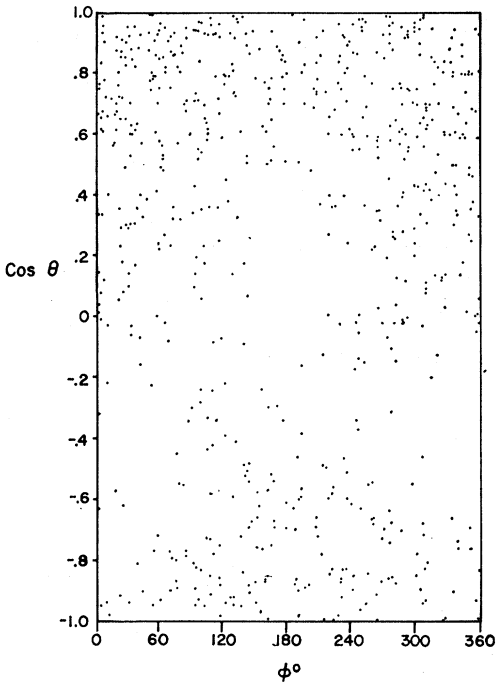

FIG. 29. Treiman-Yang angle ϕ versus the cosine of the π^- scattering angle for the $\pi^-\pi^+$ system in the mass range 0.7 to 0.8 GeV/c^2 and for $|t|<10\mu^2$.

Figure 27 shows a plot of log(number of events) vs $|t|/\mu^2$ together with a least-squares fit to a straight line which gives $d\sigma/dt=(0.36\pm0.03)e^{+(10.26\pm0.06)t}$ mb (GeV/c^2)$^{-2}$. This is very close to the ρ^- production results, differing only by the expected value (assuming

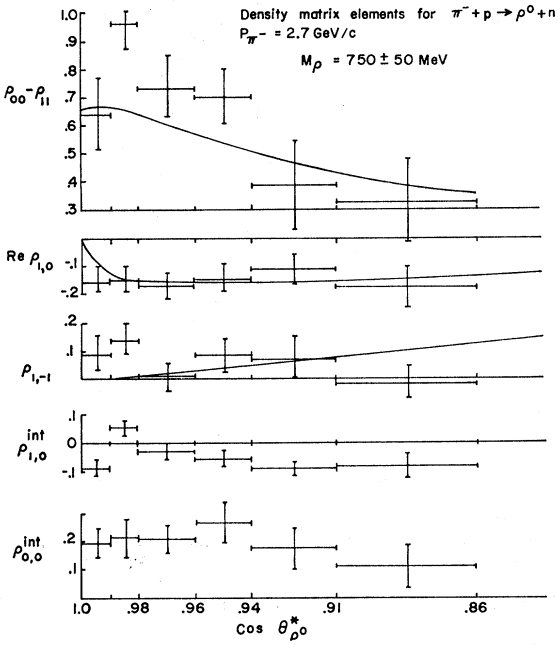

FIG. 30. Density-matrix elements as a function of cosθ^* for ρ^0 production.

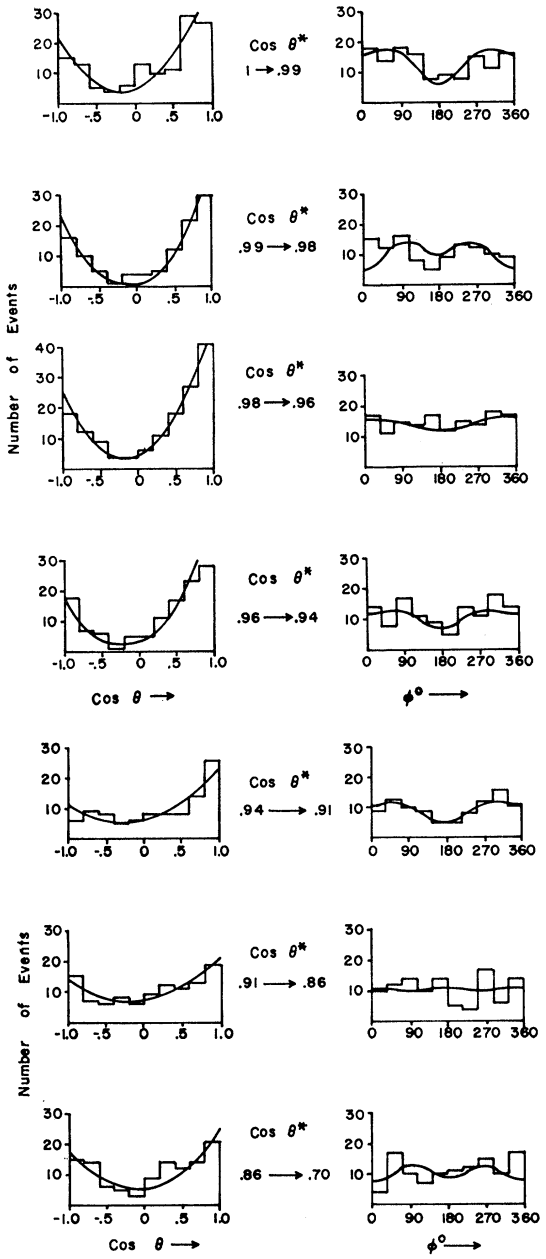

FIG. 31. Cosine of the "$\pi\pi$ scattering angle" and Treiman-Yang angle for successive intervals of $\cos\theta_{\rho^0}$* using events with $M_{\pi^-\pi^+}$ from 0.7 to 0.8 GeV/c^2.

one-pion exchange) of 2 in cross section. The asymmetry in $\cos\theta$ is displayed in Fig. 28 in terms of the asymmetry parameter $\alpha=(F-B)/(F+B)$, where F is the number of events with $\cos\theta>0$ and B is the number of events with $\cos\theta<0$. The $\pi^+\pi^-$ asymmetry shows a maximum below 700 MeV/c^2 and falls off near the ρ^0 mass in contrast to the $\pi^-\pi^0$ channel (see Fig. 22) in which α exhibits a smooth increase as a function of dipion effective mass. The dashed curve in Fig. 28 is due to Patil[12] and assumes a $T=0$, $J=0$ resonance at 700

TABLE V. Experimentally determined values of the ρ^0 and ρ^- masses, widths, and $\sigma(\rho)/\sigma(\pi\pi N)$ for different regions of $|t|$.

$\lvert t\rvert$	M (MeV)	Γ (MeV)	Fraction of ρ
		ρ^-	
$<5\mu^2$	777±6	137±17	0.91±0.05
$<10\mu^2$	775±5	145±12	0.83±0.04
$<20\mu^2$	768±5	153±13	0.74±0.04
		ρ^0	
$<5\mu^2$	771±5	160±15	0.90±0.05
$<10\mu^2$	770±5	160±15	0.87±0.04
$<20\mu^2$	770±4	160±15	0.81±0.04

MeV/c^2; the agreement is not good particularly below 600 MeV/c^2. The data are in good agreement with the solid curve which is a compilation of data from experiments at 1.6, 2.75, 3.0, and 4.5 GeV/c incident pion momenta.[35] The decay angular distribution of the ρ^0 is plotted in Fig. 29. An event was used for this analysis if $700<M_{\pi^+\pi^-}<800$ MeV/c^2 and if the four-momentum transfer squared to the nucleon was less than or equal to ten pion masses squared. In the figure the cosine of the polar angle θ is plotted against the azimuthal angle of the negative decay pion. The plot is anisotropic in both variables and asymmetric in $\cos\theta$; it shows depopulation in the middle and along two edges.

To account for the asymmetry in $\cos\theta$ a $T=0$, $J=0$ amplitude has been assumed.[11] No strong $\pi\pi$ interactions have been reported in the $T=2$ state, and the $J=2$ amplitude is enhanced only above 1 GeV.[36] Just as for the ρ^- the spin states of the $\pi^+\pi^-$ system are described by density matrix elements in the helicity representation.

For P- and S-wave amplitudes the density matrix

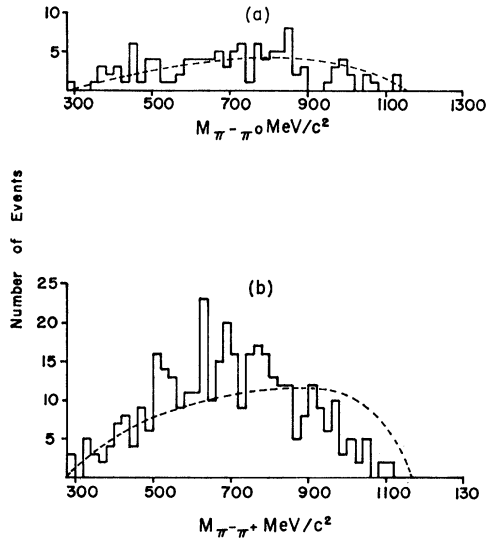

FIG. 32. The $\pi\pi$ effective-mass distributions for $|t|>140\mu^2$: (a) $\pi^-\pi^0$ from $p\pi^-\pi^0$; (b) $\pi^-\pi^+$ from $\pi^-\pi^+n$.

[35] J. P. Baton and J. Regnier, Nuovo Cimento 36, 1149 (1965).
[36] G. Wolf, Phys. Letters 19, 328 (1965).

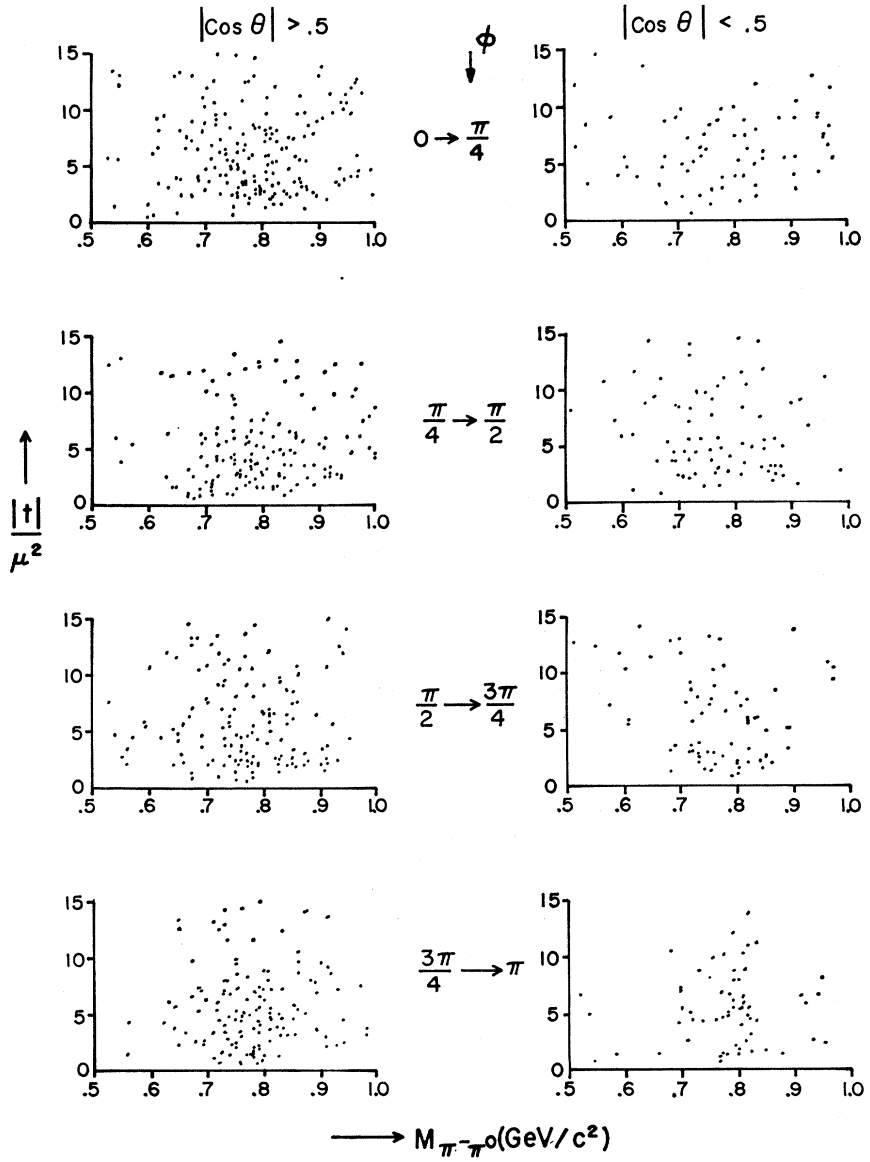

FIG. 33. Effective mass of the $\pi^-\pi^0$ system versus $|t|/\mu^2$ for different regions of the Treiman-Yang and π^- scattering angles.

becomes, assuming Hermiticity and time-reversal invariance

$$\begin{pmatrix} \rho_{11} & \rho_{10} & \rho_{1,-1} & \rho_{10}^{\text{int}} \\ \rho_{10}^{*} & \rho_{00} & -\rho_{10}^{*} & \rho_{00}^{\text{int}} \\ \rho_{1,-1} & -\rho_{10} & \rho_{11} & -\rho_{10}^{\text{int}} \\ \rho_{10}^{\text{int}*} & \rho_{00}^{\text{int}*} & -\rho_{10}^{\text{int}*} & \rho^{T=0} \end{pmatrix}.$$

The decay angular distribution is[37]

$$W(\theta,\phi)=(1/4\pi)+(3/4\pi)\{(\rho_{00}-\rho_{11})(\cos^2\theta-\tfrac{1}{3}) -2\sqrt{2}\,\mathrm{Re}\rho_{10}\sin\theta\cos\theta\cos\phi-\rho_{1,-1}\sin^2\theta\cos2\phi\} +(\sqrt{3}/4\pi)\{-2\sqrt{2}\,\mathrm{Re}\rho_{1,0}^{\text{int}}\sin\theta\cos\phi +2\,\mathrm{Re}\rho_{00}^{\text{int}}\cos\theta\}.$$

[37] P. Csonka and L. Gutay, University of California Lawrence Radiation Laboratory Report No. UCRL 50101, 1966 (unpublished).

The symbol ρ^{int} denotes the density matrix elements due to S-P wave interference. The trace condition $\sum \rho_{\mu\mu}=1$ was also imposed. The events with effective mass between $700<M_{\pi\pi}<800$ MeV/c^2 were arranged in descending order of $\cos\theta^*$ and divided into consecutive groups of about 100 events. The experimental angular distribution in θ and ϕ was fitted to the theoretical distribution, $W(\theta,\phi)$, by maximum-likelihood techniques. The results are displayed in Fig. 30. One can see that the ρ^0 and the corresponding ρ^- density matrix elements in Fig. 21 show rather similar behavior.

Assuming various models, the magnitude of the density matrix elements can be calculated. The prediction of the absorption-modified one-pion-exchange model[27] for ρ^0 production in the $J=1$ state is plotted on Fig. 30 as a solid curve for ρ_{00}, $\rho_{1,0}$, $\rho_{1,-1}$, and $\rho_{00}-\rho_{11}$.

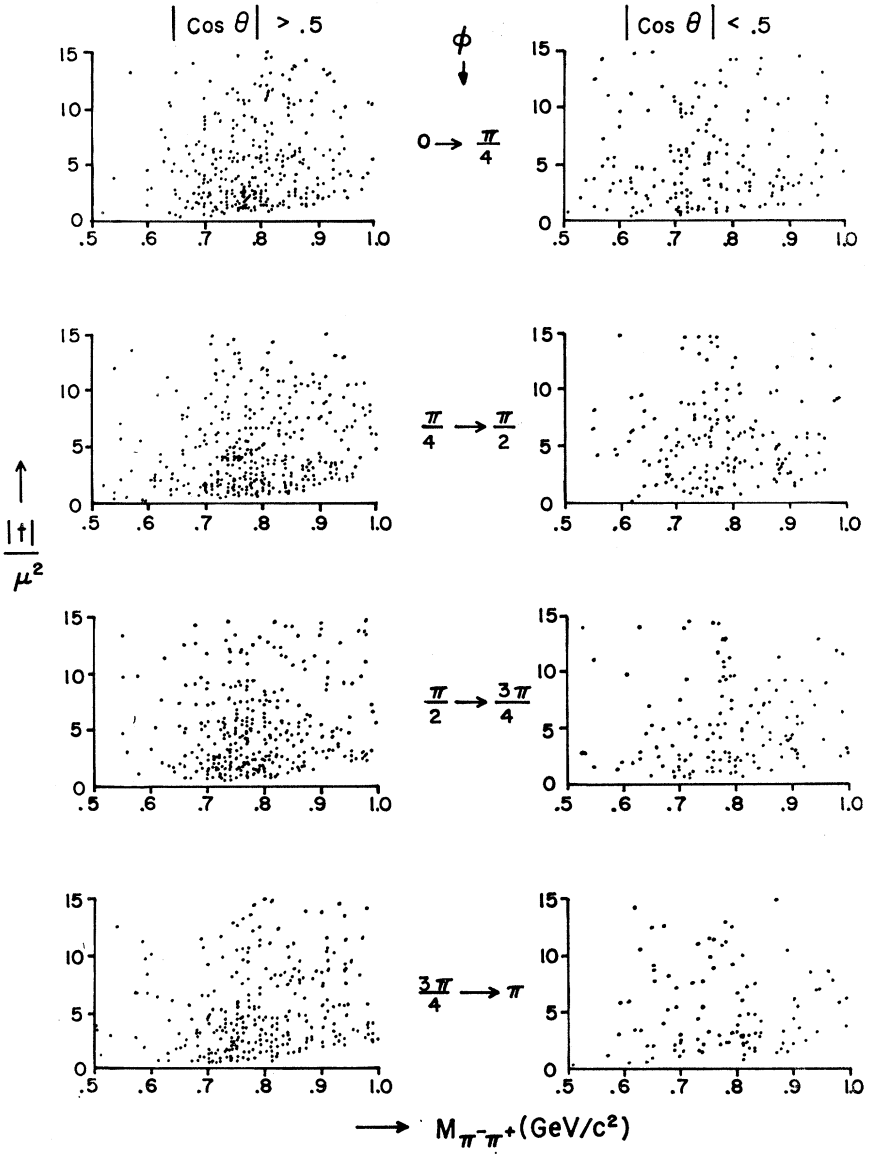

FIG. 34. Effective mass of the $\pi^-\pi^+$ system versus $|t|/\mu^2$ for different regions of the Treiman-Yang and π^- scattering angles.

We can see that the solid curves which were obtained without any S wave agree with experiment except for the $\rho_{00}-\rho_{11}$ term. It seems that around $\cos\theta^*\approx 0.99$ the absorption effects on ρ_{00} are minimized. This is in agreement with Jackson's prediction, but the value of ρ_{00} is larger than predicted. For samples with $\cos\theta^*<0.91$ a rapid decrease in the $\rho_{00}-\rho_{11}$ term is observed. The interference term ρ_{00}^{int} does not show any dramatic variations as a function of $\cos\theta^*$. The distributions in ϕ and θ alone are given by

$$U(\phi)=(1/2\pi)\{1+2\rho_{1,-1}(1-2\cos^2\phi) - (\tfrac{1}{2}\pi\sqrt{6})\,\mathrm{Re}\rho_{1,0}^{\text{int}}\cos\phi\},$$

$$V(\theta)=\tfrac{1}{2}\{1+(\rho_{00}-\rho_{11})(3\cos^2\theta-1) +2\sqrt{3}\,\mathrm{Re}(\rho_{00}^{\text{int}})\cos\theta\}.$$

The corresponding angular distributions have been plotted in Fig. 31. The solid curves for $\cos\theta$, obtained from the maximum-likelihood solutions for the two-dimensional distribution, fit the experimental θ distributions rather well. The same is true for the ϕ distributions with the exception of the intervals $0.99>\cos\theta^*>0.98$ and $0.91<\cos\theta^*<0.86$ in which the ϕ distributions are symmetric.

The angular distributions of the break up of the $\pi^-\pi^+$ system for $|t|<20\mu^2$ and in the effective-mass interval of 600–900 MeV/c^2 were fitted using Legendre polynomials. The distributions were well represented using terms up to and including $L=1$ and no evidence for higher partial waves was found. It seems unlikely therefore that the asymmetry in the shape of the ρ peak is due to higher angular-momentum states.

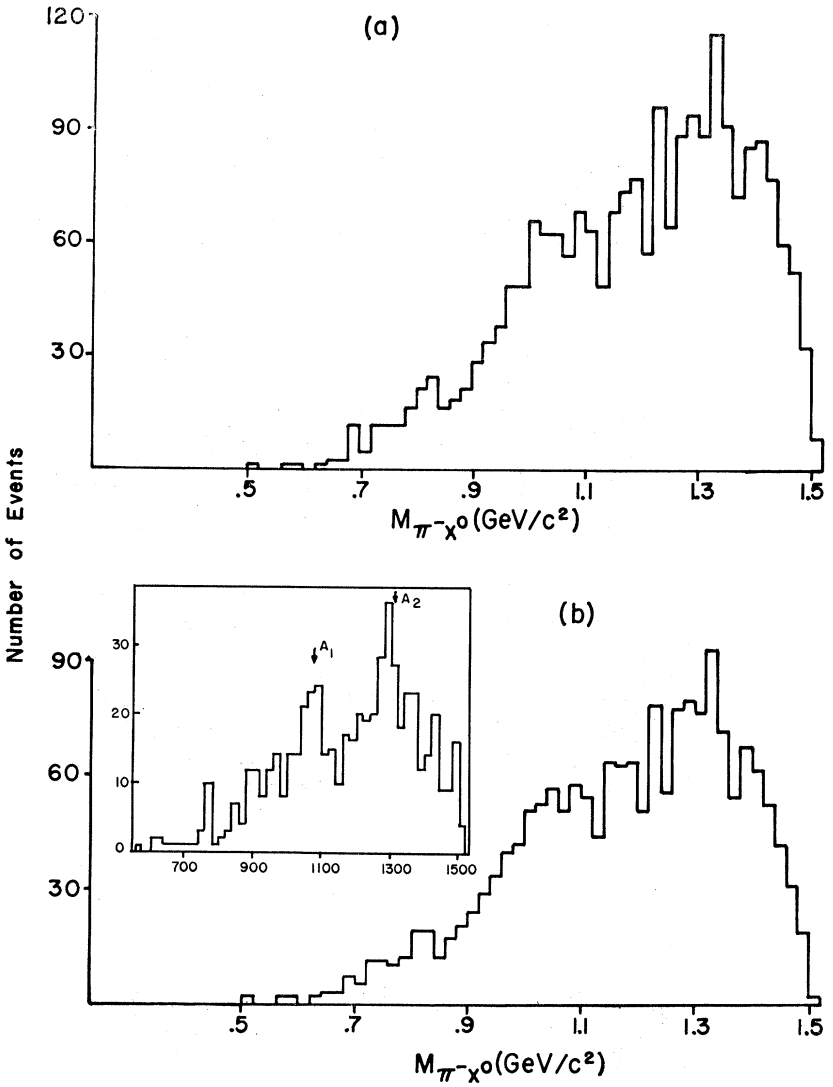

FIG. 35. (a) Effective-mass distributions of the $\pi^- X^0$ system from the final state $\pi^- p X^0$. (b) The same distribution as in (a) using just those events with four-momentum transfer squared to the proton $<40\mu^2$.

An attempt was made to determine the S- and P-wave phase shifts in these same mass and four-momentum transfer squared intervals treating the data as real $\pi\pi$ scattering. Under this assumption, the results indicate a resonant P-wave and a linearly rising S-wave term. In addition, however, there appeared to be an extra isotropic contribution which had its maximum magnitude at 780 MeV/c^2 and then decreased sharply. Similar effects were found when off-shell corrections were applied. This analysis seems to indicate that absorption effects are probably very important and an attempt is being made to include these effects in the analysis. The $\pi^-\pi^+$ effective-mass distribution was examined for $|t|<4\mu^2$ and $|\cos\theta|<0.3$ to see if any significant shift in the mass of the ρ peak occurred. A shift of the peak to 720 MeV/c^2 has been taken previously[15] as evidence for the existence of a $T=0$, $J=0$ resonance. Our data do not show any significant shift and in addition the $\pi^-\pi^0$ mass distribution appears to behave in the same way as the $\pi^-\pi^+$ distribution for various $|t|$ and $\cos\theta$ intervals.

VII. MASS AND WIDTH OF THE ρ MESON

In order to determine the experimental values of the mass and width of the ρ meson, events were used having low four-momentum transfer to the $\pi\pi$ system.

The di-pion mass distribution was fitted using maximum-likelihood techniques with a combination of phase-space and ρ-resonance production for $|t|$ less than $5\mu^2$, $10\mu^2$, and $20\mu^2$. The percentage of resonance production, the mass and width of the ρ were variables whose best values were determined from these fits. The results for the ρ^0 and ρ^- are shown in Table V and are consistent with previously determined values. The ρ^- results show a decrease in width with $|t|$ which is probably due to the decreasing effect of final-state interactions. The ρ^0 parameters show a different behavior, this being due to

an apparent excess of events above 0.85 GeV/c^2. These events caused the ρ peak to be asymmetric and a determination of its width to be subject to larger errors. These events did not appear to be associated with f^0 production or to wrongly assigned events and were probably due to some kinematical effect distorting phase space.

ρ-meson production was also looked for at high values of $|t|$ as the possibility exists of nucleon exchange processes becoming important in this region. The $\pi^-\pi^0$ and $\pi^-\pi^+$ di-pion mass histograms for $|t|>140\pi^2$ are shown in Fig. 32, the dashed line being a phase-space estimate. No clear resonance production is observed although the $\pi^-\pi^+$ distribution deviates more from phase space than the $\pi^-\pi^0$ distribution.

The ρ mass and width appears to be a function of $|t|$, $\cos\theta$ and ϕ (see Fig. 15). Figures 33 and 34 show this variation where $|t|$ versus $M\pi\pi$ plots are shown for various ranges of $\cos\theta$ and ϕ. A particular variation is seen for $|\cos\theta|<0.5$ and $3\pi/4<\phi<\pi$ where the $\pi\pi$ effective mass appears to peak at a value above that normally accepted for the ρ meson. No clear explanation has been found for this behavior.

VIII. FINAL STATE $\pi^-p\to\pi^-p+X^0$ (NEUTRALS) AND $\pi^-p\to\pi^-\pi^+ +X^0$ (NEUTRALS)

A total of 10 466 events were accepted as belonging to one of the above two reactions. Using ionization information obtained from examining each event on a scanning table, 6901 events were unambiguously assigned to the reaction $\pi^-p\to\pi^-\pi^+X^0$ (reaction 5) and 2215 events were assigned to $\pi^-p\to\pi^-pX^0$ (reaction 3). This left 1350 events having acceptable kinematics for both reactions with the positive secondary having a momentum greater than 1250 MeV/c. These events were examined and compared with the unambiguous events and it was concluded that about 70% were from reaction (5) and 30% from reaction (3). In the analysis of these reactions no additional interesting features were observed by adding this sample of 1350 to both final states. The histograms shown in Figs. 35–38, therefore, do not include this sample although it has been used for all relevant cross-section calculations.

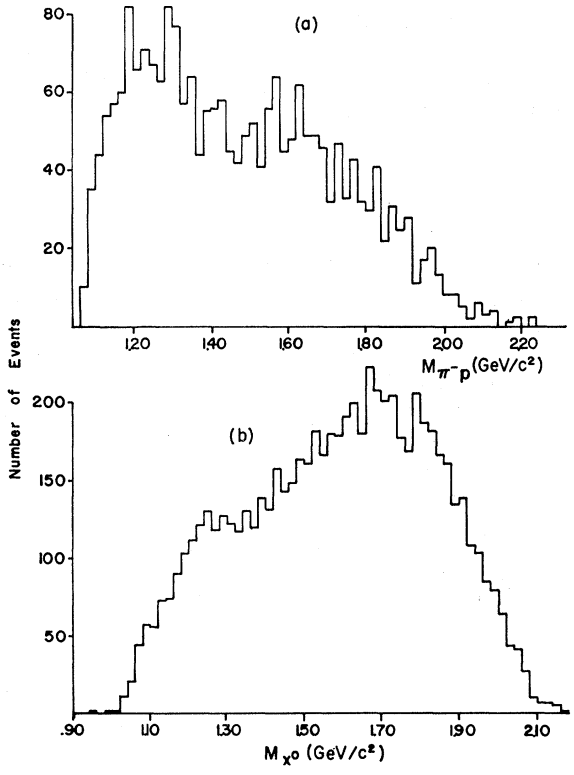

FIG. 36. (a) Effective-mass distribution of the X^0 system from the final state π^-pX^0. (b) Effective-mass distribution of the X^0 system from the final state $\pi^-\pi^+X^0$.

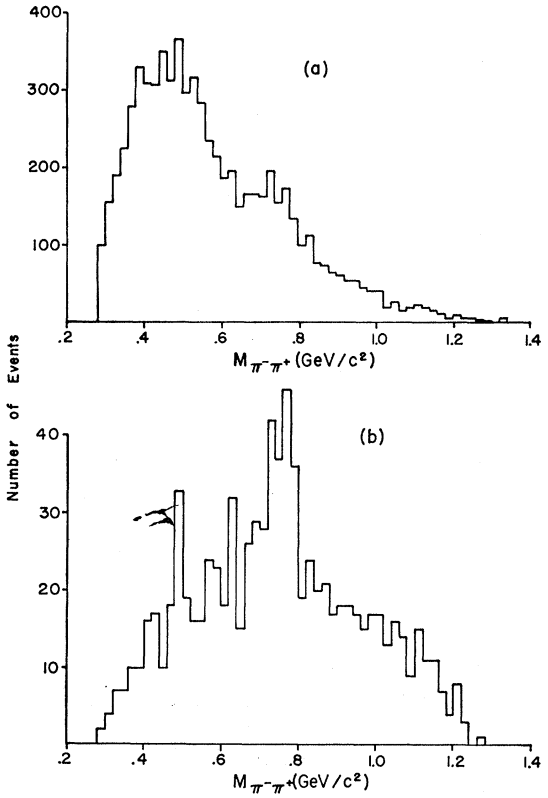

FIG. 37. (a) Effective-mass distribution of the $\pi^-\pi^+$ system from the final state $\pi^-\pi^+X^0$. (b) The same distribution as in (a) using just those events having M_{x^0} between 1.15 and 1.3 GeV/c^2.

A. Resonance Production

The effective-mass distributions of all possible combinations of particles were plotted and examined as a function of four-momentum transfer to each combination. Of particular interest in the final state $\pi^-p\to\pi^-pX^0$ is the possibility of observing the decays of the $A1$ and $A2$ mesons. A recent experiment[38] using the same final

[38] Saclay-Orsay-Bari-Bologna Collaboration, Phys. Letters **15**, 69 (1965).

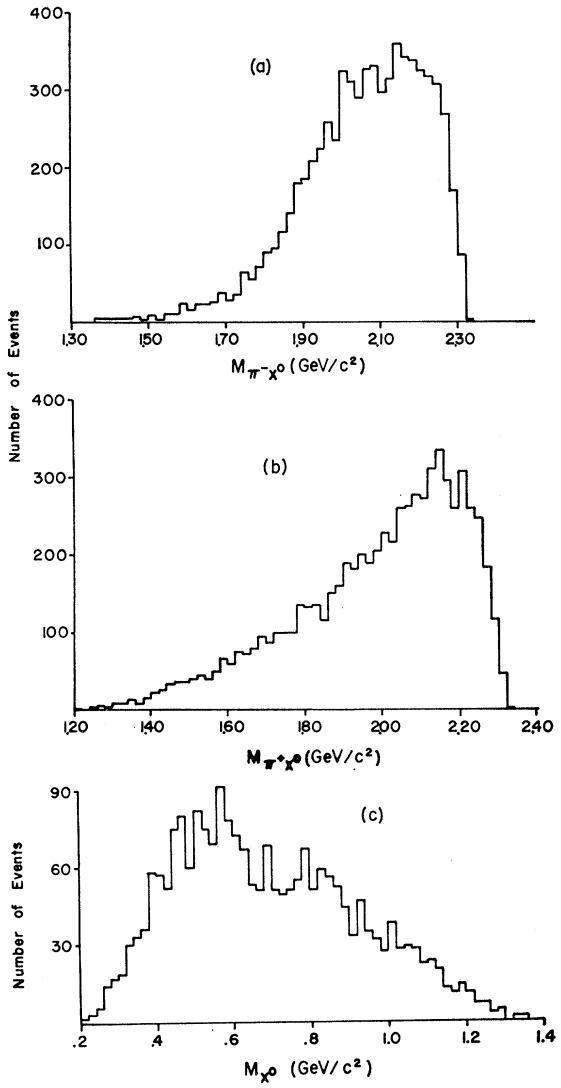

FIG. 38. Effective-mass distributions: (a) π^-X^0 system from $\pi^-\pi^+X^0$; (b) π^+X^0 system from $\pi^-\pi^+X^0$; (c) X^0 system from π^-pX^0.

state at 2.75 GeV/c has reported the observation of both $A1$ and $A2$ decays into π^-X^0. The particular histogram of interest is shown in Fig. 35 where events are plotted having $-t$ to the π^-X^0 system less than $40\mu^2$. The inset histogram shows the results of Ref. 38 and both histograms do show some kind of enhancement around 1100 and 1300 MeV/c^2. These enhancements are not so clear in our data, however, which contains about three times as many events. These enhancements are not improved by taking other cuts in the four-momentum transfer to the π^-X^0 system. In the final state $p\pi^-\pi^+\pi^-$ reported previously,[2] some evidence of $A1$ and $A2$ decay to $\rho^0\pi^-$ was observed. The enhancements in Fig. 35 are of the same order of magnitude (corresponding to $\rho^-\pi^0$ decay) but the background is too high for cross-section determination or a systematic analysis to be made. $A2$ production of this order of magnitude in these final states has been seen clearly in a recent experiment[39] and also in a compilation of π^-p interactions above 2.5 GeV/c.[40] The existence of the $A1$ as a true resonance in these final states, however, has not been definitely established.

Some of the other possible effective-mass plots are shown in Figs. 36–38 and these do exhibit indications of some $N^*(1238)$, ρ and other resonance production. The ρ production in the final state $\pi^-\pi^+X^0$ appears to be enhanced in the region where X^0 has the mass of the $N^*(1238)$. This is seen in Fig. 37 where the $\pi^-\pi^+$ effective mass is plotted for the X^0 mass between 1150–1300 MeV/c^2. It is estimated from this that the cross section for $\pi^-p \to \rho^0+N^{*0}$ ($\rho^0 \to \pi^+\pi^-$, $N^* \to n\pi^0$) is 0.15 $\pm$0.08 mb. This is in good agreement with the results for $\pi^-p \to \rho^0+N^{*0}$ ($\rho^0 \to \pi^+\pi^-$, $N^* \to p\pi^-$).

The effective-mass plot for the missing neutrals for reaction (3) is shown in Fig. 38(c). There is no clear indication of the decay of any well-defined particle and this was true even when four-momentum transfer cuts were applied to the data.

In summary, therefore, these reactions are not a fruitful source of resonance production which can be isolated and studied. It appears that resonance production does take place with small cross sections and large background.

ACKNOWLEDGMENTS

The authors wish to thank Professor J. D. Jackson for several helpful discussions and for providing them with some results of his theoretical calculations. They are also indebted to Professor F. T. Meiere, Professor A. Tubis, and Dr. P. Csonka for much useful advice. Finally, without the cooperation of members of the Alvarez group at the Lawrence Radiation Laboratory, and in particular Professor Donald H. Miller who provided the film, this work would not have been possible.

[39] F. Lefèbvres, B. Levrat, H. R. Blieden, L. Dubal, M. N. Focacci, D. Freytag, J. Geibel, W. Kienzle, B. C. Maglić, N. Martin, and J. Orear, Phys. Letters **19**, 434 (1965).

[40] T. Ferbel, Phys. Letters **21**, 111 (1966).